International Journal of Solids and Structures 125 (2017) 22–42

Contents lists available at ScienceDirect

International Journal of Solids and Structures

journal homepage: www.elsevier.com/locate/ijsolstr

Micro-based enriched multiscale homogenization method for analysis of heterogeneous materials

Hamid Bayesteh, Soheil Mohammadi*

High Performance Computing Lab, School of Civil Engineering, University of Tehran, Tehran, Iran

ARTICLE INFO

Article history:
Received 27 February 2017
Revised 8 July 2017
Available online 21 July 2017

Keywords:
Multiscale
Micro-based kinematic variable
Enrichment
Crack

ABSTRACT

The aim of this contribution is to present a multiscale framework that incorporates required spatial distribution of strain field from RVE into the macro level by adoption of appropriate enrichment functions and corresponding additional kinematic variables from the RVE level. The basic idea of macroscopic kinematic variable in advanced multiscale homogenization methods is comprehensively examined, and while the *macro-based* approach has been available in the literature, the new proposed *micro-based* scheme is explored in this study. Furthermore, the proposed approach is employed to formulate the new "Enriched MultiScale Homogenization Method (EMSHM)", based on the micro-based scheme. The key steps of adoption of appropriate additional kinematic variables, scale transition procedure and applying boundary conditions are also explained. Afterwards, EMSHM is applied to cases of cracked RVEs and severe strain gradient in the vicinity of macroscopic crack, with the inspiration of Heaviside (H-EMSHM) and crack tip (T-EMSHM) enrichments of the extended numerical methods. Accuracy of H-EMSHM with respect to the direct numerical modeling is explained with one and two dimensional examples. Numerical results of T-EMSHM have shown superior advantageous over the first order homogenization method from both the spatial distribution and magnitude of stress near the macro crack tip region.

1. Introduction

Theoretical and numerical complexities associated with new developments in different fields such as structural mechanics, aerospace, material science, bio-mechanics and chemistry have challenged the classical framework of continuum mechanics, especially in cases that several scales are involved. Accordingly, *multiscale methods* have been developed over the years to overcome the computational problems related to multiple scales in order to determine the macroscopic solution from the microscopic response, and to capture the micro behavior of material. It should be noted that the terms *micro scale* and *macro scale* are used here to represent the lower and higher scales of a multiscale solution, and they may include different length scales of a problem such as nanometer, micrometer, millimeter, etc.

Multiscale methods generally include *sequential* and *concurrent* solutions (Tadmor and Miller, 2011). In the first case, the micro problem is solved, and its results are used as input variables for the macroscopic solution. In a concurrent method, both scales are solved simultaneously, which require an appropriate correlation between the microscopic and macroscopic scales. Sequential methods are computationally more efficient than the concurrent solutions, however they usually suffer from many restrictions of the classical continuum theory.

Concurrent methods are also subdivided into the *hierarchical* and *partitioned-domain* approaches (Tadmor and Miller, 2011). In partitioned-domain methods, while the medium is generally solved with a macro level governing equation, another theory/resolution is employed to handle a particular part of the domain. In contrast, hierarchical methods consider all resolutions (from different scales) at the same time and position. Partitioned-domain methods are mostly used in cases where the classical continuum theory is violated in particular sub-regions, while hierarchical methods, also called homogenization methods, incorporate the micro level effects in the macro solution at the whole domain. Both methods can be employed in a problem simultaneously. In the present study, homogenization methods are examined and extended by adoption of new kinematic variables to allow for analysis of micro-scale discontinuities or higher gradients.

The first order homogenization is based on the classical continuum theory which assumes the locality condition, where the stress in any point is solely related to the strain at that point. To further incorporate the microscopic effects in the continuum theory, nonlocal and generalized continua theories have been devel-

* Corresponding author.
E-mail addresses: hbayesteh@ut.ac.ir (H. Bayesteh), smoham@ut.ac.ir (S. Mohammadi).

http://dx.doi.org/10.1016/j.ijsolstr.2017.07.018
0020-7683/

oped (Bažant and Jirásek, 2002). In multiscale framework, integral type nonlocal based methods are introduced nonlocal constitutive law (Tognevi et al., 2016; Yvonnet and Bonnet, 2014), and generalized continua are subdivided into higher grade and higher order theories (Forest, 2002; Fish and Kuznetsov, 2010; 2012) based on the type of incorporation of micro-effects. In higher grade theories, higher spatial derivatives (i.e. gradient of strain) are used as additional terms in the weak formulation to consider the micro effects (Fish and Kuznetsov, 2010; Kouznetsova et al., 2004), while higher order theories use additional degrees of freedom (that are explicitly introduced independent of the displacement field), e.g. micromorphic (McVeigh et al., 2006; Vernerey et al., 2007) and Cosserat (Forest and Sab, 1998; Forest et al., 1999; 2001) theories. A well review paper by Forest (2002) examines different homogenization techniques based on the continuum theory used in macro and micro levels. Among them, the first order multiscale homogenization has been vastly employed in a wide range of linear (Hassani and Hinton, 1998b; 1998a) and nonlinear simulations (Miehe, 2002), shape memory alloys (Damanpack et al., 2015) and bio-mechanics problems (Rohan et al., 2012). Furthermore, in nonlinear problems, homogenization based on the model reduction approaches were proposed to efficiently combine analytical and computational procedures (Michel and Suquet, 2016) via some simplifications. Among them, transformation field analysis (TFA) has been established by piecewise constant inelastic strain (Dvorak et al., 1994), and successfully developed to nonuniform transformation field analysis (NTFA) (Roussette et al., 2009; Michel and Suquet, 2003; 2016), assuming non-constant distribution of inelastic strain.

Despite the good agreement between the first order homogenization and reference solutions in many cases, this method should not be used in conditions where scale separation is violated, particularly in severe strain gradient and strain localization conditions inside RVE. Considerable efforts have been dedicated to enhance the multiscale homogenization. In most cases, extra variables in the form of independent degrees of freedom or higher gradient terms in the weak formulation were considered to capture special effects in micro and macro levels. In the most general case, the multiresolution approach (Liu and McVeigh, 2008; Tang et al., 2013) based on the micromorphic theory adopted 12 independent additional degrees of freedom to consider dislocation effects, softening due to shear band, etc. in RVE. Vernerey et al. (2007) showed how the multiresolution scheme could degenerate to other methods such as micromorphic, Cosserat and strain gradient models, where additional degrees of freedom could be associated with rotation and/or stretch of the underlying RVE.

The second order mutiscale computational homogenization was developed by Kouznetsova et al. (2004), based on the assumption of gradient of deformation gradient to explore strain localization in RVE, but it was incapable of considering strong localizations. Later, the homogenization method was extended to contemplate severe localization in RVE with modifying the macroscopic deformation gradient tensor (Bosco et al., 2014; 2015). In this case, the displacement discontinuity was introduced as an independent macroscopic kinematic variable, applied on RVE to resolve challenges related with the softening in RVE. Similar approaches to associate softening in RVE with the macroscopic traction-separation law of cohesive crack were proposed with different underlying assumptions due to the source of localization, RVE boundary condition, and additional constraint to hold objectivity (Nguyen et al., 2012; Coenen et al., 2012a; 2012b; Sánchez et al., 2013; Toro et al., 2014; Sánchez et al., 2011). Comprehensive discussion was presented by Sánchez et al. (2011) to express how to apply an appropriate macroscopic kinematic variable on RVE, in addition to the conventional macroscopic strain, as a framework for multiscale homogenization.

In contrast to methods that use additional independent degrees of freedom (Vernerey et al., 2007) or need C^1 continuity (Kouznetsova et al., 2004) to consider strain gradient in RVE, the computational continua approach, proposed in (Fish and Kuznetsov, 2010) and revisited in (Fish et al., 2015), introduced the variational formulation for non-constant deformation gradient based on the nonlocal quadrature integration. While this method had several advantages of the gradient formulations, it was incapable of considering nonlocal effects (Fish and Kuznetsov, 2010).

Moreover, the concept of multiscale enrichment based on the partition of unity (Fish and Yuan, 2005) was introduced to consider higher gradient approximation in a local macro crack tip domain, in which micro-fluctuations were superimposed on the standard FEM displacement field using the PU property over the macro elements and the basic functions of the asymptotic mathematical homogenization as enrichment functions.

All the mentioned multiscale methods use higher derivatives (Kouznetsova et al., 2004; Fish and Kuznetsov, 2010) or crack displacement opening (Sánchez et al., 2013; Bosco et al., 2014) of macroscopic field variable as additional terms in the weak formulation, or use independent degrees of freedom (Fish and Yuan, 2005; Vernerey et al., 2007) to represent the intended phenomena. Generally, methods that introduce additional independent degrees of freedom are more robust and flexible to deal with complex problems, despite having higher computational efforts. Accordingly, researchers have tried to use the minimum number of additional degrees of freedom, with meaningful macroscopic kinematic variables from the macro scale, along with adoption of appropriate scale transition approaches. The procedures that use additional terms from the macro scale considerations, are called the *macro-based* kinematic variable approach (in this study), and has been well explained in Sánchez et al. (2011). In contrast, the present work introduces, for the first time, a new viewpoint by defining the new kinematic variables from the microscopic phenomena in the RVE level, that is called hereafter the *micro-based* additional kinematic variable approach. The key characteristics of the new kinematic variables in the macro-based and micro-based perspectives are that they are initially associated with meaningful phenomena in macro or micro scales, respectively. It will be discussed that the new approach is more flexible and robust in developing accurate and efficient first order multiscale homogenization.

In the present study, the general framework of micro-based kinematic variables is explained and then applied to two complex problems of cracked RVE and singular strain gradient in RVE. In the next section, the first order multiscale homogenization is briefly reviewed. Then, the scale transition concepts are discussed, and the proposed enriched multiscale homogenization method (EMSHM) is introduced according to the micro-based kinematic variables. Afterwards, this framework is used to formulate cracked RVE and singular strain fields near a macroscopic crack. Different numerical examples are comprehensively examined to assess the performance of the proposed EMSHM, and to justify the concluding remarks.

2. First order multiscale homogenization

The first order homogenization, broadly investigated in the literature (e.g. (Nemat-Nasser and Hori, 1998; Miehe, 2002)), is reviewed in this section. In this method, the strain field in an RVE is the superposition of macroscopic strain $\bar{\varepsilon}_{ij}$ and complementary strain field $\tilde{\varepsilon}_{ij}$ due to the micro fluctuations in the RVE,

$$\varepsilon^{\zeta}_{ij}(\mathbf{x},\mathbf{y}) = \bar{\varepsilon}_{ij}(\mathbf{x}) + \tilde{\varepsilon}_{ij}(\mathbf{y}) \tag{1}$$

where the superscript ζ in ε^{ζ}_{ij} denotes that the strain is defined in the heterogeneous medium and is assumed to be highly oscillating. The macroscopic spatial variable $\mathbf{x}$ defines the location of RVE in the macroscopic domain and the microscopic variable $\mathbf{y}$

varies in the RVE. In the first order computational homogenization (CH1), having assumed a constant macroscopic strain on the RVE, the macroscopic quantity $\bar{\varepsilon}_{ij}(\mathbf{x})$ becomes independent of $\mathbf{y}$. In CH1, the macroscopic virtual power density field, $\delta\bar{p}(\mathbf{x})$, is a function of $\bar{\varepsilon}_{ij}(\mathbf{x})$, and is denoted by $\delta\bar{p}\big(\bar{\varepsilon}_{ij}\big)$, as (Tian et al., 2010)

$$\delta\bar{p}\big(\bar{\varepsilon}_{ij}(\mathbf{x})\big) = \frac{1}{|\Omega_\Theta|}\int_{\Omega_\Theta}\delta p(\mathbf{x},\mathbf{y})d\Omega = \frac{1}{|\Omega_\Theta|}\int_{\Omega_\Theta}\sigma_{ij}(\mathbf{x},\mathbf{y})\delta\varepsilon^{\zeta}_{ij}(\mathbf{x},\mathbf{y})d\Omega \tag{2}$$

where Ω_Θ represents the RVE domain, $|\Omega_\Theta|$ is the RVE volume, and $\delta p(\mathbf{x},\mathbf{y})$ is the virtual power density of material in the RVE. Substituting (1) into (2), the following macroscopic virtual power density is achieved

$$\delta\bar{p}\big(\bar{\varepsilon}_{ij}(\mathbf{x})\big) = \bar{\sigma}_{ij}(\mathbf{x})\delta\bar{\varepsilon}_{ij}(\mathbf{x}) \tag{3}$$

that denotes the Hill-Mandel lemma with

$$\bar{\sigma}_{ij}(\mathbf{x}) = \frac{1}{|\Omega_\Theta|}\int_{\Omega_\Theta}\sigma_{ij}(\mathbf{x},\mathbf{y})d\Omega \tag{4}$$

Additionally, condition (5) must be applied to hold Eq. (3) (Miehe, 2002)

$$\int_{\Gamma_\Theta}\tilde{u}_i(\mathbf{y})n_j d\Gamma = 0 \tag{5}$$

where Γ_Θ is the boundary of RVE, n_j is the unit normal vector on Γ_Θ and

$$\tilde{u}_{(i,j)}(\mathbf{y}) = \frac{1}{2}\big[\tilde{u}_{i,j}(\mathbf{y}) + \tilde{u}_{j,i}(\mathbf{y})\big] = \tilde{\varepsilon}_{ij}(\mathbf{y}) \tag{6}$$

Details of deriving relations (3), (4) and (5) are explained in Appendix A. Condition (5) can be applied in different ways, but in practice, appropriate boundary conditions are imposed on the RVE to ensure (5) is satisfied automatically (Miehe, 2002) that is listed in Appendix B for standard RVEs. The periodic boundary condition results in the minimum error in conventional problems (Miehe, 2002).

3. Additional kinematic variables and scale transition

First, a brief review of general procedure of the first order and more advanced multiscale computational homogenization, as the basis of macro-based kinematic variable procedure, is described, and then, the basic concepts of the developed micro-based method are explained.

3.1. Macro-based kinematic variable

In the conventional multiscale homogenization, the deformation gradient (Kouznetsova, 2002) (or equivalently the strain field in the small deformation theory) is assumed to be superposed of a kinematic macroscopic variable (e.g. deformation gradient or strain tensor) and micro-fluctuation terms due to any heterogeneity, including crack, porosity, inclusion and dislocation. In the simplest form, the macroscopic strain is constant on RVE and the strain in the micro level is defined with (1). Additionally, the boundary conditions of RVE are established with the kinematic scale-transition relation. For example, the macro-micro strain relation

$$\bar{\varepsilon}_{ij}(\mathbf{x}) = \frac{1}{|\Omega_\Theta|}\int_{\Omega_\Theta}\varepsilon^{\zeta}_{ij}(\mathbf{x},\mathbf{y})d\Omega \tag{7}$$

leads to the constraint (5) on RVE (Miehe, 2002). In more advanced homogenization methods (e.g. second-order multiscale homogenization), relation (1) is modified to include additional macroscopic terms. Accordingly, Eq. (1) can be generalized to (Sánchez et al., 2013)

$$\varepsilon^{\zeta}_{ij}(\mathbf{x},\mathbf{y}) = \bar{\varepsilon}_{ij}(\mathbf{x}) + \Im(\chi_1,\chi_2,\ldots) + \tilde{\varepsilon}_{ij}(\mathbf{y}) \tag{8}$$

where $\chi_i (i = 1,2,\ldots)$ represent additional macroscopic variables and $\Im$ is an operator in terms of χ_i. Different additional macroscopic variables χ_i are introduced to modify the classical homogenization method, such as the gradient of deformation gradient (Kouznetsova, 2002) and the macroscopic crack opening displacement (Sánchez et al., 2013; Bosco et al., 2014). Operator $\Im$ is adopted based on the selected additional macroscopic variables. Subsequently, an appropriate scale transition procedure should be adopted as an extra constraint due to the selection of additional kinematic variables. This procedure leads to new boundary conditions on RVE, as comprehensively explained in Sánchez et al. (2013) for the case of material failure analysis in this framework.

After introducing the macroscopic kinematic variables in the multiscale computational homogenization, the work conjugate of each macroscopic kinematic variable is defined using the Hill-Mandel condition, introduced in Eq. (2). This principle leads to the macroscopic stress (4) in the first order homogenization. In the general case of (8), the appropriate work conjugate of each additional macroscopic variable, χ_i is extracted using the macro-micro strain energy equality, as explained in Kouznetsova (2002) for the second order homogenization and Sánchez et al. (2013) for the cohesive crack.

Briefly, the general procedure employed in the macro-based kinematic variable methods can be described as:

- Step 1. Defining the microscopic strain field with the superposition of macroscopic variables (including strain/deformation gradient and additional terms with appropriate operators) and the micro-fluctuation field, Eq. (8).
- Step 2. Defining the scale-transition procedure to relate the macroscopic kinematic variables to the microscopic displacement field (e.g. Eq. (7)).
- Step 3. Applying the appropriate boundary conditions to solve RVE with the help of operator defined in Stp1 and relations obtained in Step2 (e.g. constraint (5)).
- Step 4. Extraction of macroscopic work conjugate variable of each macroscopic kinematic variable from the Hill–Mandel principle (e.g. Eq. (4)).

One of the most important aspects of developing the first order multiscale homogenization is *the way additional kinematic variables should be selected* in Step 1 to obtain better results. These additional terms are adopted according to the problem in hand and the phenomena which are taking place in the macroscopic domain. The basic framework of this procedure is to consider the macroscopic variables that are ***already*** *meaningful in the* ***macroscopic*** *scale*. It means that the meaning of the kinematic macroscopic variables are already known from the macro (and NOT micro) continuum model. For example, in addition to the macro strain (deformation gradient), the well-known macroscopic variables are the strain gradient (gradient of deformation gradient) and crack opening (in failure modeling). Accordingly, the relationship between macro and micro kinematic variables can be found based on the scale-transition kinematic operator. This perspective is demonstrated in Fig. 1a.

3.2. Micro-based kinematic variable

As mentioned earlier, adoption of kinematic variable is a key step in developing an efficient multiscale method. In contrast to the existing macro-based approach, in this paper, the kinematic variables that are *predefined* and meaningful in the *microscopic* scale, emanate from the micro-scale to determine the response of

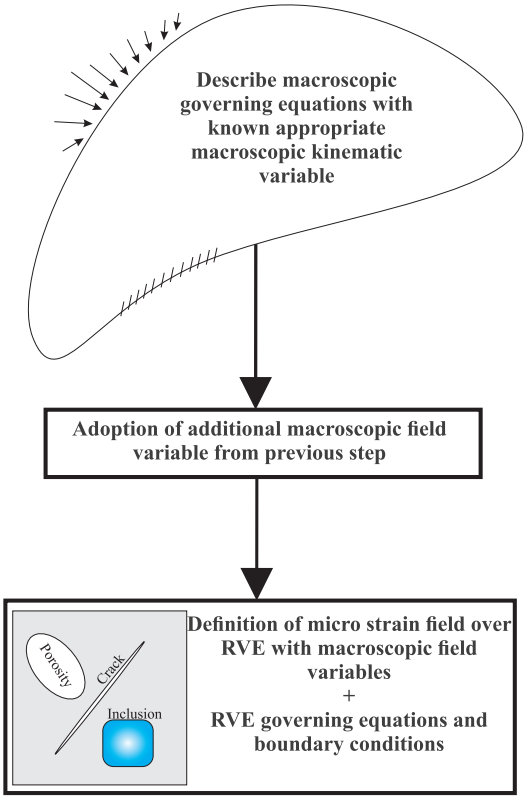

(a) macro-based procedure to consider macroscopic kinematic variable and to derive microscopic governing equations.

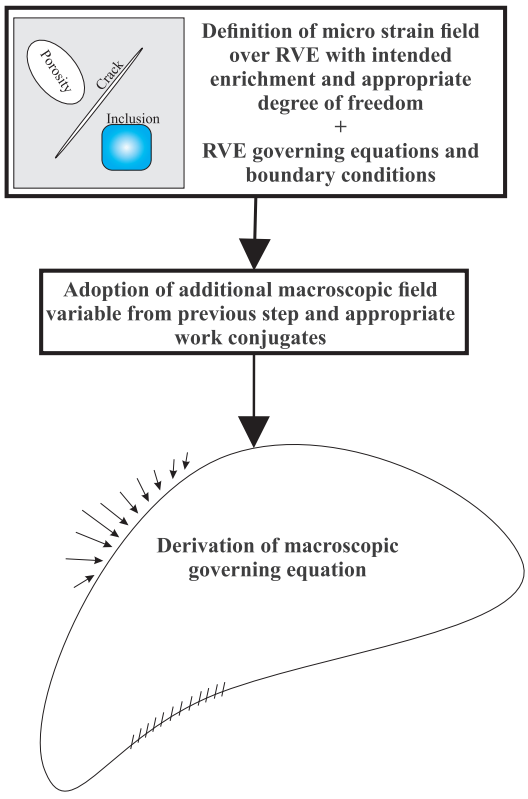

(b) micro-based procedure to adopt new macroscopic kinematic variable and to derive macroscopic governing equations.

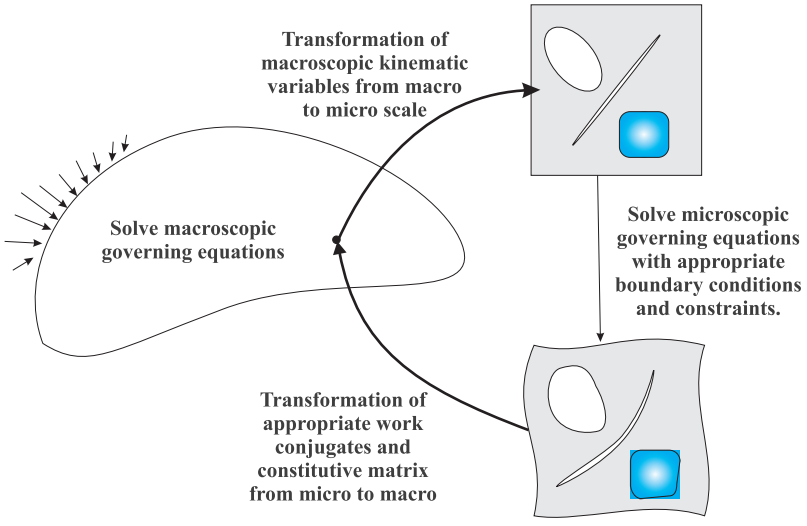

(c) iteration procedure for solving coupled macro and micro governing equations in both micro-based and macro-based viewpoints.

Fig. 1. Micro and macro based procedure of adopting macroscopic additional kinematic variable and solution procedure.

equivalent macro homogeneous material. This framework allows for better interpretation of the final macroscopic kinematic variables and different boundary conditions on RVE and is expected to be more versatile in capturing complex phenomena such as softening, shear-band, dislocation, etc. within the RVE. This viewpoint is demonstrated in Fig. 1b.

It is important to note the difference between the mathematical homogenization based on the multiscale asymptotic expansion (Fish et al., 1994) and the multiscale computational homogeniza-

tion (Kouznetsova et al., 2004) methods to highlight the macro and micro based concepts. In the mathematical homogenization, the substantial goal is to find that "*Is there any macroscopic governing equation whose response is the leading term of the multiscale asymptotic expansion?*", while the aim of the multiscale computational homogenization is "*to find the response of the macroscopic stress by solving the RVE located at a macroscopic point subjected to the macroscopic kinematic variable*". While both methods lead to apparently identical formulation for the first order case, they are different in concept (Nemat-Nasser and Hori, 1998), and result in different formulations for higher order cases. In the proposed micro-based approach, the main idea is to enrich macro continuum level using the additional kinematic variables that are *directly* derived from the RVE level. Accordingly, the general framework to develop a new multiscale method, called *Enriched MultiScale Homogenization Method (EMSHM)*, is now presented.

4. Enriched Multiscale homogenization method (EMSHM)

In this section the general framework and formulation of EMSHM are explained. Two more practical applications of this method, the case of a singular strain gradient near a macroscopic crack tip and the effect of crack within RVE on the macro scale response are further developed and discussed.

4.1. Microscopic governing equations

In the enriched multiscale homogenization method (EMSHM), the macroscopic strain energy depends not only on the macroscopic strain, but also to the additional terms associated with a particular phenomenon in RVE. As mentioned in the previous section, the fundamental differences of EMSHM with other available multiscale methods is in the concept and approach of determining these additional terms that leads to the present interpretation of enriched macroscopic variables and boundary conditions, which provides a powerful and more versatile basis for analysis of complex problems that cannot be accurately solved by the first order multiscale homogenization approach.

As mentioned earlier, the strain field in RVE in the first order multiscale homogenization is expressed with $\varepsilon_{ij}^{\zeta}(\mathbf{x},\mathbf{y}) = \bar{\varepsilon}_{ij}(\mathbf{x}) + \tilde{\varepsilon}_{ij}(\mathbf{y})$ and the macroscopic virtual power density $\delta\bar{p}\left(\bar{\varepsilon}_{ij}\right)$ depends on $\bar{\varepsilon}_{ij}$. The strain field in EMSHM is also written with the same approach, but based on *a macro continuum material whose virtual power density, δp^M, depends on not only $\bar{\varepsilon}_{ij}(\mathbf{x})$, but also $\tilde{\varepsilon}_{ij}(\mathbf{y})$*; $\left(\delta p^M\left(\bar{\varepsilon}_{ij},\tilde{\varepsilon}_{ij}\right)\right)$. Notation δp^M is adopted here to distinguish between macroscopic virtual power density in the first order multiscale homogenization and EMSHM. Having written the complementary strain field $\tilde{\varepsilon}_{ij}(\mathbf{y})$ in RVE, the effects of complex phenomena such as singular terms are included in the macroscopic virtual power density. Accordingly,$\delta p^M\left(\bar{\varepsilon}_{ij},\tilde{\varepsilon}_{ij}\right)$ can be expressed as,

$$\delta p^M\left(\bar{\varepsilon}_{ij},\tilde{\varepsilon}_{ij}\right) = \delta\bar{p}\left(\bar{\varepsilon}_{ij}\right) + \delta\tilde{p}\left(\tilde{\varepsilon}_{ij}\right) \tag{9}$$

Additionally, $\tilde{\varepsilon}_{ij}$ is decomposed into the enhanced strain ε_{ij}^{*} and symmetric displacement gradient $u_{(i,j)}^{1}$ components,

$$\tilde{\varepsilon}_{ij} = \varepsilon_{ij}^{*} + u_{(i,j)}^{1} \tag{10}$$

Substituting (10) into (1), the total variation of the strain field is expressed with

$$\delta\varepsilon_{ij}^{\zeta} = \delta\bar{\varepsilon}_{ij} + \delta\varepsilon_{ij}^{*} + \delta u_{(i,j)}^{1} \tag{11}$$

It is noted that almost the same expression was reported in Sánchez et al. (2011) for superposition of macro and micro scale strain fields. However, the additional term in Sánchez et al. (2011) was related to the macroscopic phenomena (e.g. macroscopic crack). The differences will become clearer in the fallowing discussions. Furthermore, ε_{ij}^{*} in (10) can be defined on the whole RVE domain, Ω_{Θ}, or on any subpart of RVE domain, Ω_{Θ^*}, where $\Omega_{\Theta^*} \subset \Omega_{\Theta}$.

Noting that the enhanced part, ε_{ij}^{*}, of the complementary strain field $\tilde{\varepsilon}_{ij}$ comes, as an additional independent kinematic variable, from RVE to macro homogeneous medium, only ε_{ij}^{*} should be used to determine the macroscopic virtual power density. Accordingly, $\tilde{p}\left(\tilde{\varepsilon}_{ij}\right)$ is replaced with $p^*\left(\varepsilon_{ij}^{*}\right)$ and Eq. (9) is modified to

$$\delta p^M\left(\bar{\varepsilon}_{ij},\tilde{\varepsilon}_{ij}\right) = \delta\bar{p}\left(\bar{\varepsilon}_{ij}\right) + \delta p^*\left(\varepsilon_{ij}^{*}\right) \tag{12}$$

To define an equivalent homogeneous material, its macroscopic virtual power density should be equal to the volume average of the virtual work exerted on RVE,

$$\begin{aligned}\delta p^M\left(\bar{\varepsilon}_{ij},\varepsilon_{ij}^{*}\right) &= \delta\bar{p}\left(\bar{\varepsilon}_{ij}\right) + \delta p^*\left(\varepsilon_{ij}^{*}\right)\\ &= \frac{1}{|\Omega_{\Theta}|}\int_{\Omega_{\Theta}} \sigma_{ij}(\mathbf{x},\mathbf{y})\delta\varepsilon_{ij}^{\zeta}(\mathbf{x},\mathbf{y})d\Omega\end{aligned} \tag{13}$$

Substituting (11) into (13),

$$\begin{aligned}\delta\bar{p}\left(\bar{\varepsilon}_{ij}\right) + \delta p^*\left(\varepsilon_{ij}^{*}\right) &= \frac{1}{|\Omega_{\Theta}|}\int_{\Omega_{\Theta}} \sigma_{ij}\left(\delta\bar{\varepsilon}_{ij} + \delta\varepsilon_{ij}^{*} + \delta u_{(i,j)}^{1}\right)d\Omega\\ \Rightarrow &\left[\delta\bar{p}\left(\bar{\varepsilon}_{ij}\right) - \frac{1}{|\Omega_{\Theta}|}\int_{\Omega_{\Theta}} \sigma_{ij}\delta\bar{\varepsilon}_{ij}d\Omega\right]\\ &+\left[\delta p^*\left(\varepsilon_{ij}^{*}\right) - \frac{1}{|\Omega_{\Theta}|}\int_{\Omega_{\Theta}} \sigma_{ij}\delta\varepsilon_{ij}^{*}d\Omega\right]\\ &+\left[-\frac{1}{|\Omega_{\Theta}|}\int_{\Omega_{\Theta}} \sigma_{ij}\delta u_{(i,j)}^{1}d\Omega\right] = 0\end{aligned} \tag{14}$$

Considering that $\delta\bar{p}$ and δp^* are functions of just $\bar{\varepsilon}_{ij}$ and ε_{ij}^{*}, respectively, the following three basic equations are obtained from the fundamental lemma of variational calculus

$$\delta\bar{p}\left(\bar{\varepsilon}_{ij}\right) = \frac{1}{|\Omega_{\Theta}|}\int_{\Omega_{\Theta}} \sigma_{ij}\delta\bar{\varepsilon}_{ij}d\Omega = \left(\frac{1}{|\Omega_{\Theta}|}\int_{\Omega_{\Theta}} \sigma_{ij}d\Omega\right)\delta\bar{\varepsilon}_{ij} = \bar{\sigma}_{ij}\delta\bar{\varepsilon}_{ij} \tag{15a}$$

$$\delta p^*\left(\varepsilon_{ij}^{*}\right) = \frac{1}{|\Omega_{\Theta}|}\int_{\Omega_{\Theta}} \sigma_{ij}\delta\varepsilon_{ij}^{*}d\Omega \tag{15b}$$

$$\frac{1}{|\Omega_{\Theta}|}\int_{\Omega_{\Theta}} \sigma_{ij}\delta u_{(i,j)}^{1}d\Omega = 0 \tag{15c}$$

Eqs. (15a) and (15b) define the macroscopic stress work conjugates of kinematic variables $\bar{\varepsilon}_{ij}$ and ε_{ij}^{*}. Comprehensive explanation of (15b) will be discussed later. The fundamental assumption in (15a) is that the macroscopic strain $\bar{\varepsilon}_{ij}(\mathbf{x})$ is constant on RVE. Consequently, the macroscopic stress $\bar{\sigma}_{ij}$ is equivalent to the volume average of stress on RVE

$$\bar{\sigma}_{ij}(\mathbf{x}) = \frac{1}{|\Omega_{\Theta}|}\int_{\Omega_{\Theta}} \sigma_{ij}(\mathbf{x},\mathbf{y})d\Omega \tag{16}$$

which is analogous to (4) for the first order multiscale homogenization. Furthermore, (15c) defines the governing weak form equation on the RVE to compute the micro-fluctuation field $\delta u_i^1(\mathbf{y})$. Appropriate boundary conditions are necessary to solve Eq. (15c) and to obtain objective results with respect to the size of RVE.

The constraint derived in the first order multiscale homogenization is not sufficient in EMSHM due to the existence of additional kinematic variables. Different methods have been reported in the literature to modify microscopic boundary conditions based on the additional macro-based kinematic terms, however they cannot be used in the present micro-based formulation. In

EMSHM, the required boundary conditions are directly derived in Section 4.2 based on simultaneous satisfaction of equilibrium equation and relation (15c).

Remark 1. A relation similar to (12) is used in other advanced multiscale formulations, but with the key difference that in this work $\delta p^{\star}$ is not expressed in terms of the macroscopic kinematic variables and should be determined based on the enhanced kinematic variables from the RVE level in EMSHM. Moreover, a clear difference in the proposed formulation is in the definition of additional kinematic variable ε^{*}_{ij} in (11).

4.2. RVE boundary conditions

The strong form of static equilibrium equation on the RVE level in the absence of body forces is expressed as,

$$\sigma_{ij,j} = 0 \tag{17a}$$

$$\sigma_{ij} = c_{ijkl}\varepsilon^{\zeta}_{kl} \tag{17b}$$

$$\varepsilon^{\zeta}_{kl} = u^{\zeta}_{(k,l)} = \frac{1}{2}\left(u^{\zeta}_{k,l} + u^{\zeta}_{l,k}\right) \tag{17c}$$

Having utilized the weighted residual method, the following weak form is obtained from the divergence theorem,

$$\int_{\Omega_\Theta} w_i \sigma_{ij,j} d\Omega = 0 \qquad \forall w_i \in \mathbf{H}^1(\Omega_\Theta)$$

$$\Rightarrow \int_{\Omega_\Theta} w_{i,j}\sigma_{ij} d\Omega - \int_{\partial\Theta} w_i \sigma_{ij} n_j d\Gamma = 0 \qquad \forall w_i \in \mathbf{H}^1(\Omega_\Theta) \tag{18}$$

where the vector space $\mathbf{H}^1(.)$ encompasses functions whose first derivative is square-integrable. Considering the subspace $\mathbf{W}^1 \subset \mathbf{H}^1(\Omega_\Theta)$ similar to $\mathbf{V}^1$, the space of all possible functions of $u^1_i(\mathbf{y})$ in relation (15c), Eq. (18) is also hold as

$$\int_{\Omega_\Theta} w^1_{i,j}\sigma_{ij} d\Omega - \int_{\partial\Theta} w^1_i \sigma_{ij} n_j d\Gamma = 0 \qquad \forall w_i \in \mathbf{W}^1 \tag{19}$$

Knowing that $\delta u^1_{(i,j)} = w^1_{(i,j)}$ from Eq. (15c) and (19), and comparing (15c) and (19) leads to the following constraint on $u^1_i(\mathbf{y})$

$$\int_{\partial\Theta} \delta u^1_i \sigma_{ij} n_j d\Gamma = 0 \tag{20}$$

In simple problems, this constraint can be satisfied automatically using a number of appropriate boundary conditions such as periodic or minimal kinematic boundary conditions (Miehe and Koch, 2002).

4.3. Algorithm of EMSHM

The general steps of EMSHM algorithm are defined as:

- Step 1. Defining the microscopic strain field in RVE with superposition of the macro strain and complementary strain field, Eq. (11).
- Step 2. Expressing the macroscopic virtual power density based on the macroscopic strain and micro-based additional kinematic variable(s), Eq. (12).
- Step 3. Describing the macroscopic stress work conjugates of all kinematic variables, based on Eq. (15a) and (15b).
- Step 4. Solving the microscopic governing equation, Eq. (15c), with the appropriate boundary conditions, constraint (20).
- Step 5. Describing the macroscopic governing equation using the macroscopic virtual power density (12).

This procedure is adopted to formulate H-EMSHM and T-EMSHM in the next sections.

5. Heaviside enriched multiscale homogenization method (H-EMSHM)

One of the important remaining issues in the first order multiscale homogenization is to incorporate a softening behavior within RVE into the macroscopic response. In this section, EMSHM is further developed to allow for softening due to cohesive/adhesive cracks in RVE into a macro continuum model by introducing the additional kinematic variable. The macroscopic stress work conjugate of this additional kinematic variable is also computed.

5.1. Extraction of the enhanced kinematic variable in H-EMSHM

To extract ε^{*}_{ij} in (10), the strain field $\tilde{\varepsilon}_{ij}(\mathbf{y})$ in RVE should be defined. Considering the XFEM approximation in RVE, the displacement field $\tilde{u}_i(\mathbf{y})$ can be expressed as (Goli et al., 2014; Hosseini et al., 2013)

$$\tilde{u}_i(\mathbf{y}) = \sum_{k=1}^{n_{stn}} N_k \hat{u}^k_i + \sum_{k=1}^{n_{en}} N_k [H(\xi(\mathbf{y})) - H(\xi(\mathbf{y}_k))]\hat{a}^k_i \tag{21}$$

with

$$H(\xi) = \begin{cases} 1 & \xi > 0 \\ 0 & \xi < 0 \end{cases} \tag{22}$$

and

$$\xi(\mathbf{y}) = sign\left(\left(\mathbf{y} - \mathbf{y}_{\Gamma_C}\right).\vec{n}_{\Gamma_C}\right) \tag{23}$$

where Γ_C is the crack path, $\mathbf{y}_{\Gamma_C}$ is the projection of $\mathbf{y}$ on Γ_C and $\vec{n}_{\Gamma_C}$ is the unit normal vector on Γ_C, as depicted in Fig. 2. Furthermore, $\hat{u}^k_i$ and $\hat{a}^k_i$ in (21) are the standard and enriched nodal degrees of freedom, respectively (superscript k and subscript i in $\hat{u}^k_i$ and $\hat{a}^k_i$ refer to the node number and displacement component, respectively), n_{stn} is the number of nodes, n_{en} is the number of enriched nodes, and $\mathbf{y}_k$ is the position of node k.

It is proved that (21) can be rewritten as (see Appendix C)

$$\tilde{u}_i(\mathbf{y}) = (H(\mathbf{y}) - \varphi(\mathbf{y}))\beta_i + u^1_i(\mathbf{y}) \tag{24}$$

where $\varphi(\mathbf{y})$ is a smooth function, defined by (C.4) in Appendix C. One dimensional representation of $H(.)$ and $\varphi(.)$ are schematically depicted in Fig. 3.

β_i in (24) is a constant displacement jump, defined as,

$$\beta_i = \frac{1}{|\Gamma_C|}\int_{\Gamma_C} [\![\tilde{u}_i]\!] d\Gamma \tag{25}$$

where $[\![\tilde{u}_i(\mathbf{y})]\!]$ is the displacement jump of $\tilde{u}_i$ at point $\mathbf{y}$ located on Γ_C

$$[\![\tilde{u}_i(\mathbf{y})]\!] = \lim_{\Delta\mathbf{y}\to 0}(\tilde{u}_i(\mathbf{y}+\Delta\mathbf{y}) - \tilde{u}_i(\mathbf{y}-\Delta\mathbf{y})); \quad \mathbf{y} \in \Gamma_C \text{ and } \Delta\mathbf{y} \text{ is parallel to } \vec{\mathbf{n}}_{\mathbf{\Gamma_C}} \tag{26}$$

Assumption (25) allows for obtaining the constraint (27) on u^1_i in (24)

$$\int_{\Gamma_C} [\![u^1_i]\!] d\Gamma = 0 \tag{27}$$

which can be conveniently proved with substitution of (24) into (25)

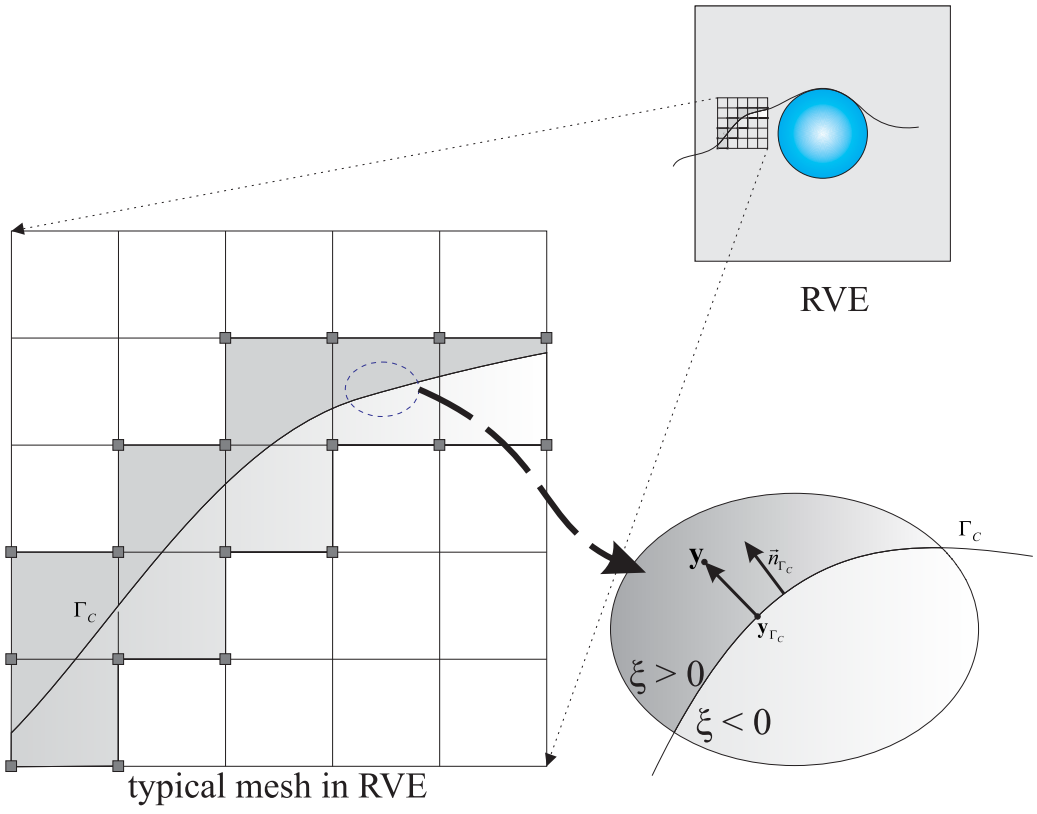

Fig. 2. Definition of the Heaviside function, and XFEM discretization in RVE.

$$\begin{aligned}\beta_i &= \frac{1}{|\Gamma_C|}\int_{\Gamma_c}[\![\tilde{u}_i]\!]d\Gamma \\ &= \frac{1}{|\Gamma_C|}\int_{\Gamma_c}\left[\!\left[(H(\mathbf{y})-\varphi(\mathbf{y}))\beta_i + u_i^1(\mathbf{y})\right]\!\right]d\Gamma \\ &= \underbrace{\frac{1}{|\Gamma_C|}\int_{\Gamma_c}[\![(H(\mathbf{y})-\varphi(\mathbf{y}))\beta_i]\!]d\Gamma}_{=\beta_i} + \frac{1}{|\Gamma_C|}\int_{\Gamma_c}\left[\!\left[u_i^1(\mathbf{y})\right]\!\right]d\Gamma \\ &\Rightarrow \int_{\Gamma_c}\left[\!\left[u_i^1(\mathbf{y})\right]\!\right]d\Gamma = 0\end{aligned} \tag{28}$$

Definition of β_i in (25) leads to the simple condition (27) that allows to set the micro displacement jump *weakly* equal to zero (i.e. the displacement jump is not zero for every point on the crack face, but its average is zero along the crack surface). The complementary strain $\tilde{\varepsilon}_{ij}$ is derived from (24),

$$\tilde{\varepsilon}_{ij} = \delta_{\Gamma_C}\left(n_j\beta_i\right)^{sym} - \left(\varphi_{,j}\beta_i\right)^{sym} + u^1_{(i,j)} \tag{29}$$

where $(\square)^{sym}$ is the symmetric part of $(\square)$, and δ_{Γ_C} is the Dirac delta function with respect to Γ_C, that is equal to one on Γ_C and vanishes along the normal to the crack line. This definition leads to the following property for arbitrary function $g(\mathbf{x})$ (Bosco et al., 2014),

$$\int_\Omega \delta_{\Gamma_C} g(\mathbf{x})d\Omega = \int_{\Gamma_C} g(\mathbf{x})d\Gamma \tag{30}$$

Combining (29) with (10) and (1), the strain field in RVE is obtained

$$\varepsilon^{\zeta}_{ij} = \bar{\varepsilon}_{ij} + \delta_{\Gamma_C}\left(n_j\beta_i\right)^{sym} - \left(\varphi_{,j}\beta_i\right)^{sym} + u^1_{(i,j)} \tag{31}$$

and comparing (29) with (10), the enhanced strain is expressed with

$$\varepsilon^*_{ij} = \delta_{\Gamma_C}\left(n_j\beta_i\right)^{sym} - \left(\varphi_{,j}\beta_i\right)^{sym} \tag{32}$$

Remark 2. It should be emphasized that Eq. (27) does not mean u_i^1 is a continuous function. It is shown in Appendix C that u_i^1 is also a discontinuous function within the XFEM discretization.

Remark 3. The enhanced strain in (32) is obtained from the decomposition of (21) in the form of (24). Other forms of decompositions or higher order terms can be considered to enhance the accuracy of this method.

Remark 4. It is important to note that β_i in (31) is not a macroscopic crack opening. It is in fact an average of microscopic crack openings, and is applied on crack faces in RVE. This is one of the substantial contrasts between the macro-based and micro-based viewpoints. It will be shown that even if there is not a macro-crack in the EMSHM problem, β_i may emerge in all macroscopic (Gauss) points whose corresponding RVEs are cracked.

Remark 5. Eq. (29) is apparently analogous to the embedded-discontinuity formulation (Oliver et al., 2006). However, they differ in concept because $u^1_{(i,j)}$ is also discontinuous in this equation. Consequently Eq. (29) represents the strain field of XFEM, as explained in Appendix C.

5.2. Enhanced stress

The work conjugate of the enhanced strain, called hereafter as the *enhanced stress*, γ_i, is expressed by

$$\gamma_i = \frac{1}{|\Omega_\Theta|}\int_{\Omega_\Theta} -\varphi_{,j}\sigma_{ij}\mathrm{d}\Omega + \frac{1}{|\Omega_\Theta|}\int_{\Gamma_C}\sigma_{ij}n_j\mathrm{d}\Gamma \tag{33}$$

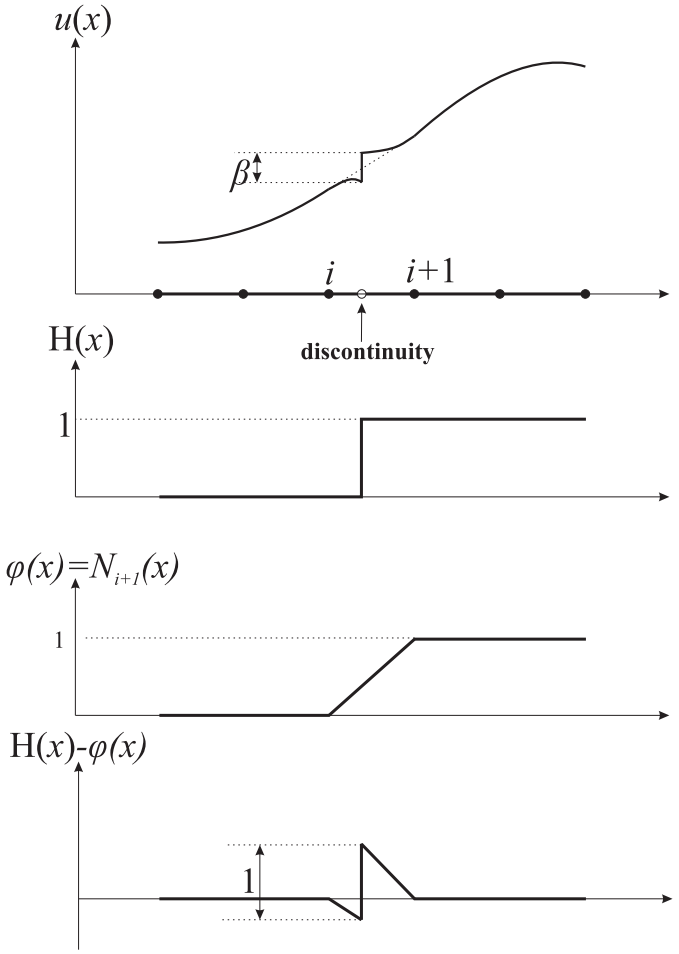

Fig. 3. One dimensional representation of $H(.)$ and $\varphi(.)$ in relation (24) based on the finite element discretization.

and the enhanced part of macroscopic power virtual density in (12) can be written as,

$$\delta p^* = \gamma_i \delta \beta_i \tag{34}$$

The term $\sigma_{ij} n_j$ in the second integral of (33) is equivalent to the cohesive traction on Γ_C. Eqs. (33) and (34) can be proved with substituting (32) into (15b)

$$\begin{aligned}
\delta p^*_{\text{int}}\left(\delta \varepsilon^*_{ij}\right) &= \delta p^*\left(\varepsilon^*_{ij}\right) \\
&= \frac{1}{|\Omega_\Theta|}\int_{\Omega_\Theta} \delta \varepsilon^*_{ij}\sigma_{ij} d\Omega \\
&= \frac{1}{|\Omega_\Theta|}\int_{\Omega_\Theta} \delta\left(\delta_{\Gamma_C}\left(n_j\beta_i\right)^{sym} - \left(\varphi_{,j}\beta_i\right)^{sym}\right)\sigma_{ij} d\Omega \\
&= \frac{1}{|\Omega_\Theta|}\int_{\Omega_\Theta} \delta_{\Gamma_C}\sigma_{ij} n_j \delta\beta_i d\Omega + \frac{1}{|\Omega_\Theta|}\int_{\Omega_\Theta} -\varphi_{,j}\sigma_{ij}\delta\beta_i d\Omega \\
&= \frac{\delta\beta_i}{|\Omega_\Theta|}\int_{\Gamma_C} \sigma_{ij} n_j d\Omega + \frac{\delta\beta_i}{|\Omega_\Theta|}\int_{\Omega_\Theta} -\varphi_{,j}\sigma_{ij} d\Omega \\
&= \underbrace{\left(\frac{1}{|\Omega_\Theta|}\int_{\Gamma_C} \sigma_{ij} n_j d\Omega + \frac{1}{|\Omega_\Theta|}\int_{\Omega_\Theta} -\varphi_{,j}\sigma_{ij} d\Omega\right)}_{\gamma_i}\delta\beta_i \\
&= \gamma_i \delta\beta_i
\end{aligned} \tag{35}$$

5.3. Microscopic governing equations and boundary conditions

From Eqs. (19) and (20), the equilibrium equation on RVE is expressed by

$$\int_{\Omega_\Theta} w^1_{i,j}\sigma_{ij} d\Omega = 0 \qquad \forall w_i \in \mathbf{W}^1 \tag{36}$$

and the constraints are applied using Eqs. (20) and (28)

$$\int_{\partial\Theta} u^1_i \sigma_{ij} n_j d\Gamma = 0 \tag{37a}$$

$$\int_{\Gamma_C} \left[\!\left[u^1_i\right]\!\right] d\Gamma = 0 \tag{37b}$$

where Γ_C and $\partial\Theta$ in (37) are clearly distinguished in Fig. 4a. Due to the existence of discontinuity in RVE, Eq. (36) is efficiently solved with the XFEM approximation (C.6b).

5.4. Macroscopic governing equation

The macroscopic governing equations of the equivalent homogeneous domain is derived in this section.

5.4.1. Virtual internal power

Substituting (34) and (15a) into (12), the macroscopic virtual power density is expressed by

$$\delta p^M\left(\bar{\varepsilon}_{ij}, \beta_i\right) = \bar{\sigma}_{ij}\delta\bar{\varepsilon}_{ij} + \gamma_i\delta\beta_i \tag{38}$$

Integrating the macroscopic virtual power density of the macro-homogeneous material, (12), over Ω (depicted in Fig. 4b), the virtual internal power, δP_{int}, is obtained from

$$\delta P_{\text{int}} = \int_\Omega \delta p^M\left(\bar{\varepsilon}_{ij}, \bar{\varepsilon}_{ij}\right) d\Omega \tag{39}$$

and substituting (38) into (39), the virtual internal power of H-EMSHM is written as,

$$\delta P_{\text{int}} = \int_\Omega \left(\bar{\sigma}_{ij}\delta\bar{\varepsilon}_{ij} + \gamma_i\delta\beta_i\right) d\Omega \tag{40}$$

5.4.2. Virtual external power

The virtual external power includes surface and body terms acting on Ω and Γ_t respectively, as depicted in Fig. 4b. A generalized body force B_i, which is resulted from the traction on crack surfaces in the RVE is also introduced. The final form of the virtual external power is expressed by

$$\delta P_{ext} = \int_\Omega (b_i\delta\bar{u}_i + B_i\delta\beta_i) d\Omega + \int_{\Gamma_t} t_i\delta\bar{u}_i d\Gamma \tag{41}$$

where t_i is the traction on the surface and $\bar{u}_{(i,j)} = \bar{\varepsilon}_{ij}$.

Remark 6. The body force B_i represents the effect of micro (RVE) crack face tractions on the body force of macro level. For a crack face traction vector q_i in the RVE level, the term $B_i\delta\beta_i$ can be defined as the virtual work of traction on crack surface divided by the RVE volume, which represents the virtual work per unit volume due to body force of a point in the macro level.

$$B_i\delta\beta_i = \frac{1}{|\Omega_\Theta|}\int_{\Gamma_C} q_i\delta\beta_i d\Gamma \tag{42}$$

The generalized traction force (analogous to the generalized body force B_i) does not appear in (41) due to the fact that the traction on crack faces in RVE does not contribute to RVE boundaries.

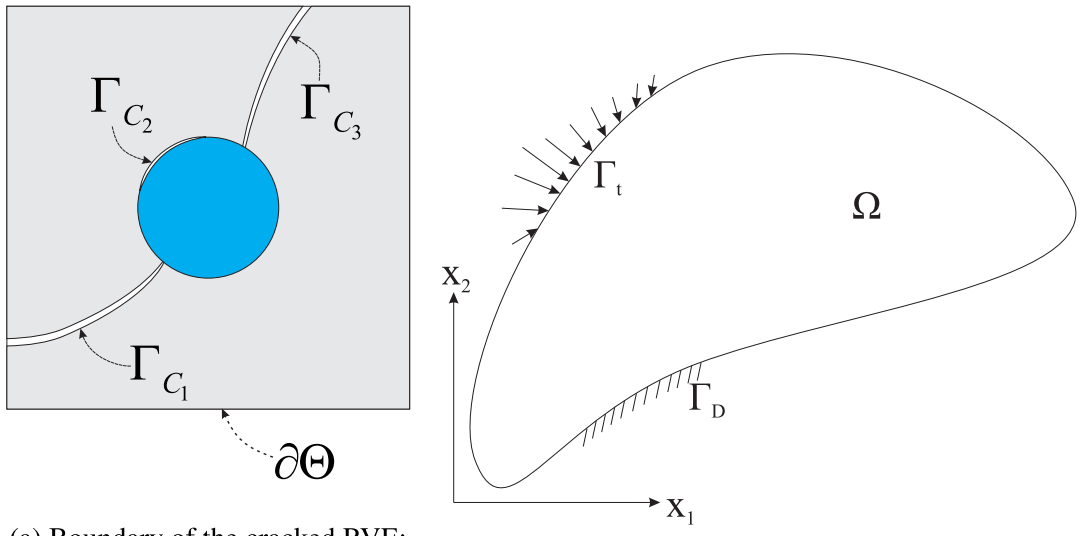

(a) Boundary of the cracked RVE:

$$\Gamma_C = \Gamma_{C_1} \cup \Gamma_{C_2} \cup \Gamma_{C_3}$$

and $\Gamma_\Theta = \Gamma_C \cup \partial\Theta$

(b) Macro homogeneous domain

Fig. 4. Schematic depiction of cracked RVE and macroscopic boundary conditions.

5.4.3. Principle of virtual work and governing equations

According to the principle of virtual work, the virtual internal and external works are in equilibrium for any independent virtual $\delta\bar{u}_i$ and $\delta\beta_i$

$$\delta P_{\text{int}} - \delta P_{ext} = 0 \tag{43}$$

Substituting (40) and (41) into (43), the weak form of macroscopic governing equations is obtained

$$\int_\Omega \left(\bar{\sigma}_{ij}\delta\bar{\varepsilon}_{ij} + \gamma_i\delta\beta_i\right)d\Omega - \int_\Omega (b_i\delta\bar{u}_i + B_i\delta\beta_i)d\Omega - \int_{\Gamma_t} t_i\delta\bar{u}d\Gamma = 0 \tag{44a}$$

$$\bar{u}_i(\mathbf{x}) = \bar{u}_i^d \qquad \mathbf{x} \in \Gamma_D \tag{44b}$$

where (44a) is true for any variation of $\delta\bar{u}_i$ and $\delta\beta_i$, and $\bar{u}_i^d$ in (44b) is the prescribed displacement on Γ_D, as depicted in Fig. 4b. Solution algorithm to solve coupled macro and micro governing equations is explained in Appendix E.

Remark 7. One of the advantages of this method is the fact that the properties of continuous and discontinuous parts in the macroscopic domain are calculated at the same Gauss points, so no additional Gauss points on the macroscopic crack are necessary.

5.5. Numerical examples of H-EMSHM

In this section, 1D and 2D numerical examples are studied based on the proposed formulation in Section 5. First, a 1D heterogeneous bar, with a weak bond between materials in RVE is considered. Afterward, a 2D multiscale problem with cracked RVEs is examined.

5.5.1. 1D heterogeneous bar

A 1D heterogeneous bar, as depicted in Fig. 5, is investigated. The bar is fixed at one end and is subjected to prescribed displacement at the other end. The RVE includes two material types with E_1 and E_2 modules of elasticity and the volume fractions $\alpha < 1$ and $(1-\alpha)$, respectively.

A traction-separation constitutive law, as depicted in Fig. 6, is considered for the spring weak bond between materials of the model. In the first part of Fig. 6, the force in spring increases linearly with the stiffness k until $d = d_0$. Afterwards, the force in spring reduces according to

$$f(d) = f_0\left|\left(\frac{d-d_0}{d_1-d_0} - 1\right)^n\right| \tag{45}$$

where parameters d_0, d_1 and f_0 are described in Fig 6.

First, this example is investigated with the following data:

$L = 5 \quad (cm)$ $\quad A = 1 \quad (cm^2)$ $\quad l = \Omega_\Theta = 1 \quad (cm)$

$\alpha = 0.5$ $\quad E_1 = 200 \quad (GPa)$ $\quad E_2 = 5 \quad (GPa)$

$k = 450 \quad \left(\frac{KN}{cm}\right)$ $\quad d_0 = 0.01 \quad (cm)$ $\quad d_1 = 0.128 \quad (cm)$

$P_0 = 4.5 \quad (KN)$ $\quad n = 2$ $\quad -$

where A is the cross section area of the bar. A direct numerical analysis (DNA) with 21 elements is used to verify the model. Fig. 7 compares the results of H-EMSHM and DNA analysis, which shows identical responses not only in the hardening part, but also in the post-peak softening segment.

To investigate the effect of volume fraction of materials in the RVE, the $f-\Delta$ curves for different values of fraction parameter α are presented in Fig. 8. It is observed that higher volume fractions lead to higher stiffness in the $f-\Delta$ curve. Furthermore, due to the nature of 1D problem, the maximum force in all conditions is limited to the maximum load of spring, $P_0 = 4.5KN$.

5.5.2. 2D heterogeneous plate with cracked RVE

In this section, a heterogeneous plate under tension and shear deformation is investigated with H-EMSHM. The constituent material is a matrix reinforced with stiff inclusions, as depicted in Fig. 9. Material properties for the matrix and inclusion are denoted by m and I, respectively.

To verify the model, the material properties are assumed as: $E_m = 68.9\,GPa$, $E_I = 379.2\,GPa$ and $\nu_m = \nu_I = 0.33$. The volume fraction $\alpha = \frac{|\Omega_I|}{|\Omega_\Theta|} = 0.0616$, where $|\Omega_I|$ is the volume of inclusion, is used in this model. Dimensions of the plate are $\frac{W}{H} = \frac{3}{7}$, and its

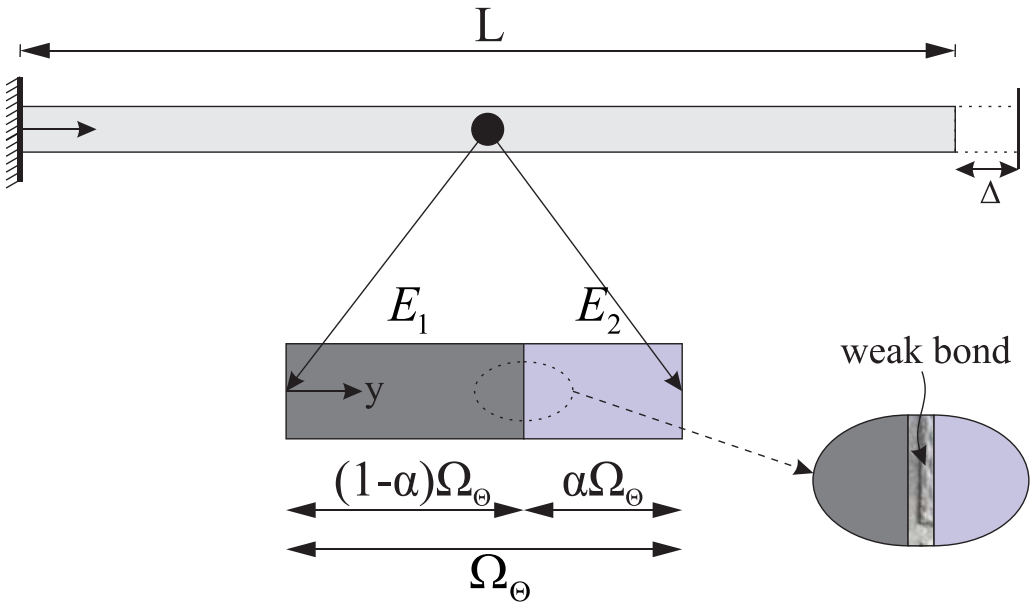

Fig. 5. 1D heterogeneous bar with weak material bonding inside the RVE.

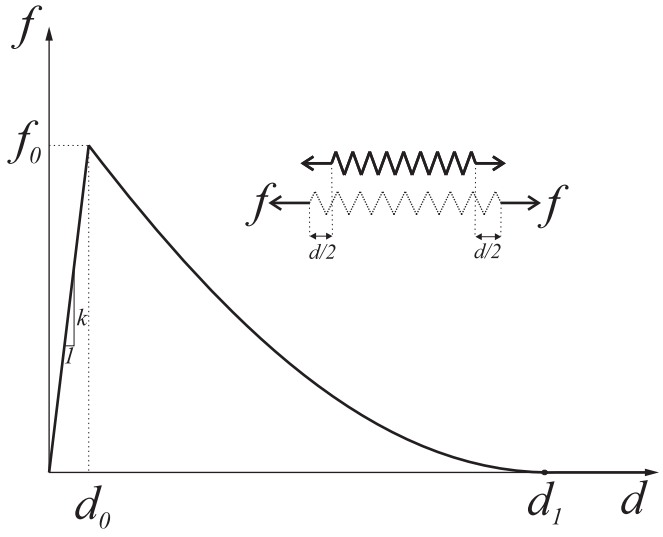

Fig. 6. Traction-separation law for the spring.

Table 1
Responses of Type-A and Type-B loadings on the 2D reinforced plate.

Type	Δ_h	Δ_v	error (%)
A	0	0.05	0.27
B	0.05	0	1.56

bottom edge is restrained against moving in horizontal and vertical directions. 442 and 21 quadrilateral elements are used to model RVE and macro-problem, respectively, as depicted in Fig. 10.

Numerical deformation of RVE under unit values of macroscopic kinematic variables $\bar{\varepsilon}_{11}$, $\bar{\varepsilon}_{22}$, $\bar{\varepsilon}_{12}$, β_1 and β_2 are depicted in Fig. 11. To verify the model, a direct numerical model containing 9450 nodes is used as the benchmark with the mesh configuration of Fig. 12. Two loading types of A and B are assumed, representing tension and shear deformations of the plate, as depicted in Figs. 13a and 13 b, respectively.

Table 2
Comparison of the normalized average stress for different ratio of $\frac{E_L}{E_m}$ in the 2D plate under prescribed displacement. ($\bar{\sigma}_{22} = \frac{\int_{\Gamma^{top}} \sigma_{22}(\mathbf{x})d\Gamma}{W}$ and $E^* = \sqrt{E_l E_m}$).

$\frac{E_L}{E_m}$	$\frac{\bar{\sigma}_{22}}{E^*}$ (present method)	$\frac{\bar{\sigma}_{22}}{E^*}$ (DNA)	error (%)
1	0.609	0.608	0.38
2	0.524	0.522	0.35
3	0.438	0.437	0.33
4	0.385	0.384	0.30
5	0.347	0.346	0.28
6	0.319	0.318	0.26
7	0.296	0.296	0.25
8	0.278	0.278	0.23
9	0.263	0.262	0.23
10	0.250	0.249	0.22

Table 3
Comparison of the normalized average stress for different number of macro elements. $E_m = 68.9GPa$, $E_l = 379.2GPa$, ($\bar{\sigma}_{22} = \frac{\int_{\Gamma^{top}} \sigma_{22}(\mathbf{x})d\Gamma}{W}$ and $E^* = \sqrt{E_l E_m}$).

Case	Number of elements	$\frac{\bar{\sigma}_{22}}{E^*}$	error with respect to case 4 (%)
1	$3 \times 7 = 21$	0.3320	0.40
2	$6 \times 14 = 84$	0.3312	0.15
3	$12 \times 28 = 336$	0.3308	0.04
4	$24 \times 56 = 1344$	0.3307	-

The results of simulations are compared in Table 1. The error, computed with respect to the direct simulation, shows a good agreement between the present method and the reference solution. Moreover, different ratios of $\frac{E_m}{E_l}$ are examined in Table 2 for the loading Type-A to investigate its effect on the model response. Values in Table 2 are average of stress $\bar{\sigma}_{22} = \frac{\int_{\Gamma^{top}} \sigma_{22}(\mathbf{x})d\Gamma}{W}$ on the top edge, normalized by $E^* = \sqrt{E_l E_m}$. Furthermore, the normalized average stress is depicted in Fig. 14 for different volume fractions α.

Additionally, to investigate the effect of number of elements, the results for four different number of elements (21, 84, 336 and 1344) are compared in Table 3 for the Type A loading. It is observed that while the results converge to the one associated with the finest mesh, the errors remain in an acceptable range.

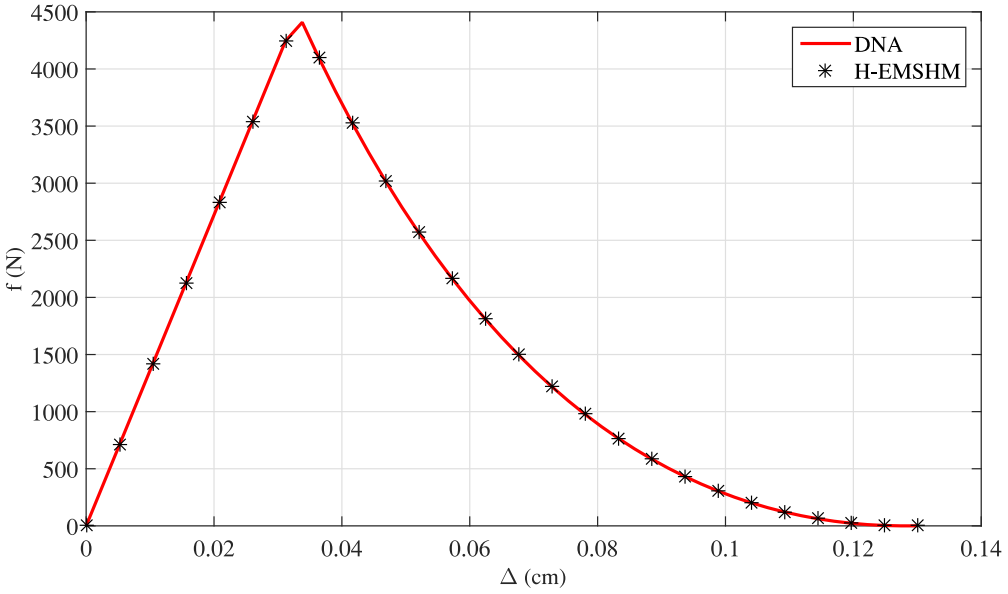

Fig. 7. Comparison of $f - \Delta$ response of 1D-bar subjected to prescribed displacement at its end for H-EMSHM and DNA.

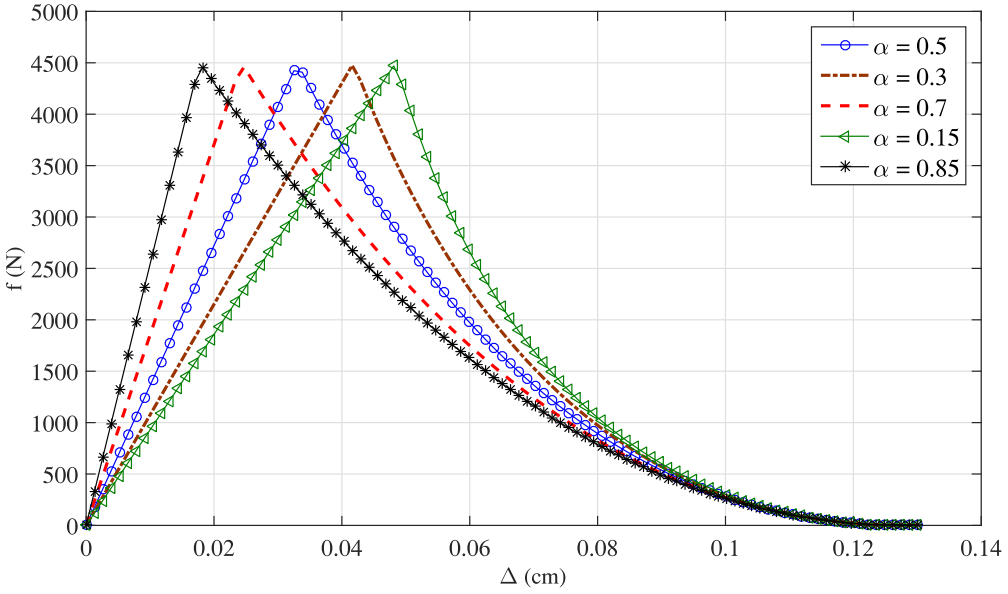

Fig. 8. $f - \Delta$ response of 1D-bar using H-EMSHM subjected to prescribed displacement for different volume fractions α.

6. Crack tip enriched multiscale homogenization method (T-EMSHM)

One of the mostly addressed shortcomings of the first order multiscale homogenization method is its assumption of constant macro strain on RVE, which limits its application to high macro strain gradient problems. Higher order theories alleviate this problem with incorporating a higher order stress field in the formulation. Furthermore, Fish and coworkers developed a novel framework based on the partition of unity concept to enrich a local region using first (Fish and Yuan, 2005) and second (Fish and Yuan, 2007) terms of the multiscale asymptotic expansion in the mathematical homogenization theory.

The singular strain field in the vicinity of a crack tip is an important case in which not only the first order homogenization assumption is violated, but also the gradient terms are insufficient to predict an accurate response. A number of techniques such as the partitioned domain based multiscale methods (Vernerey and Kabiri, 2014), were developed in atomistic and continuum levels to address this problem.

In this paper, based on a priori known $1/\sqrt{r}$ singular strain field near a crack tip (where r is the distance from the crack tip), and inspired by the extended numerical methods (Bayesteh and Mohammadi, 2013; Bayesteh et al., 2015), crack tip enrichment basis functions are employed to describe the displacement approximation in RVE to capture the effect of singular strain in the macro formulation based on the proposed EMSHM. This type of enhancement is now called T-EMSHM, considering the use of XFEM tip enrichment in the formulation.

6.1. Extraction of the enhanced kinematic variable in T-EMSHM

As mentioned in Section 4, it is necessary to properly define ε^* in EMSHM. Based on the order of singularity of the strain filed around a crack tip, the crack tip enrichment function $\sqrt{r}sin(\theta/2)$ is employed here to describe the complementary displacement field

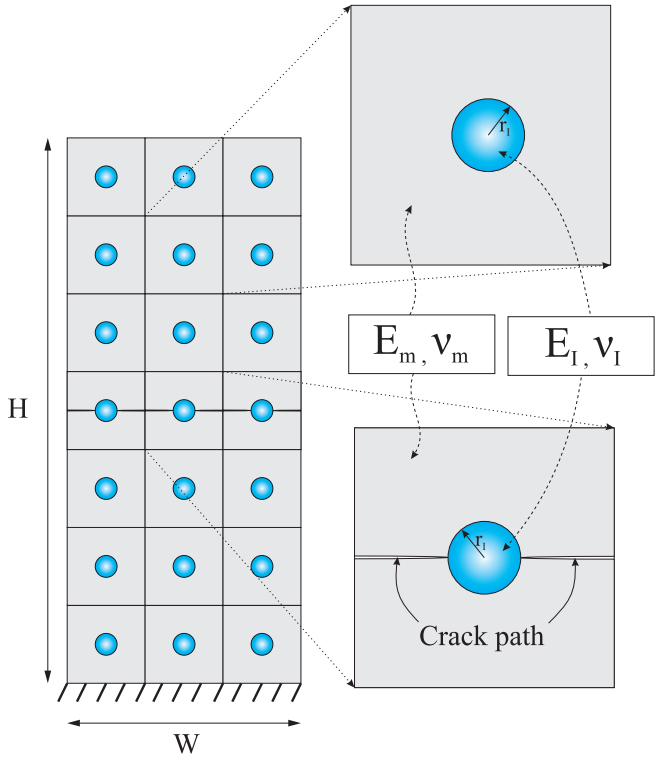

Fig. 9. 2D heterogeneous plate with cracked RVE.

with,

$$\tilde{u}_i(\mathbf{y}) = u_i^h(\mathbf{y}) + F_{ik}\alpha_k(\mathbf{y}) \tag{46}$$

where $u_i^h(\mathbf{y})$ is the standard finite element displacement field. $\alpha_k(\mathbf{y})$ is the unknown displacement field whose basis functions satisfy the partition of unity rule (Mohammadi, 2012), and F_{ik} is the enrichment function, defined by,

$$F_{ik} = f^{enr}(\mathbf{x})\delta_{ik} \tag{47}$$

where

$$f^{enr}(\mathbf{x}) = \sqrt{r}\sin\left(\frac{\theta}{2}\right) \tag{48}$$

r and θ in (48) are the local polar crack tip coordinate axes, as described in Fig. 15, and δ_{ik} is the Kronecker delta. For additional advantages of the term $\sqrt{r}sin(\theta/2)$ refer to Bayesteh et al. (2015). Furthermore, the enriched term $F_{ik}\alpha_k(\mathbf{y})$ is used over the whole domain of RVE, Ω_Θ, due to its small dimensions.

The complementary strain field is then derived as

$$\tilde{\varepsilon}_{ij}(\mathbf{y}) = \tilde{u}_{(i,j)}(\mathbf{y}) = u^h_{(i,j)}(\mathbf{y}) + F_{ik}\alpha_{(k,j)}(\mathbf{y}) + F_{(ik,j)}\alpha_k(\mathbf{y}) \tag{49}$$

where

$$u^h_{(i,j)} = \frac{u^h_{i,j} + u^h_{j,i}}{2} \tag{50a}$$

$$\alpha_{(k,j)} = \frac{\alpha_{k,j} + \alpha_{j,k}}{2} \tag{50b}$$

$$F_{(ik,j)} = \frac{F_{ik,j} + F_{jk,i}}{2} \tag{50c}$$

Details of derivation of (49) are presented in Appendix D. While the singular trend in (46) is captured by the enrichment function F_{ik}, α_k acts as a non-singular function over the RVE. Assuming a linear variation for α_k

$$\alpha_k(\mathbf{y}) \approx \bar{\alpha}_k + \bar{\alpha}^{\nabla}_{k,l} y_l \tag{51}$$

where $\bar{\alpha}_k$ and $\bar{\alpha}^{\nabla}_{k,l}$ are the magnitude of α_k and its gradient at the center of RVE. Accordingly, the symmetric gradient of α_k is obtained from (51)

$$\begin{aligned}\alpha_{(k,j)} &= \frac{\alpha_{k,j} + \alpha_{j,k}}{2} \\ &\approx \frac{\bar{\alpha}^{\nabla}_{k,l} y_{l,j} + \bar{\alpha}^{\nabla}_{j,l} y_{l,k}}{2} = \frac{\bar{\alpha}^{\nabla}_{k,l}\delta_{lj} + \bar{\alpha}^{\nabla}_{j,l}\delta_{lk}}{2} = \frac{\bar{\alpha}^{\nabla}_{k,j} + \bar{\alpha}^{\nabla}_{j,k}}{2} = \bar{\alpha}^{\nabla}_{(k,j)} \\ &\Rightarrow \alpha_{(k,j)} \approx \bar{\alpha}^{\nabla}_{(k,j)}\end{aligned} \tag{52}$$

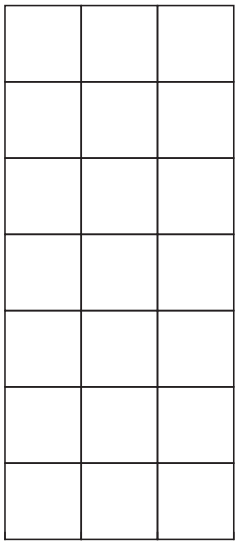

(a) Mesh configuration of macroscopic homogeneous domain

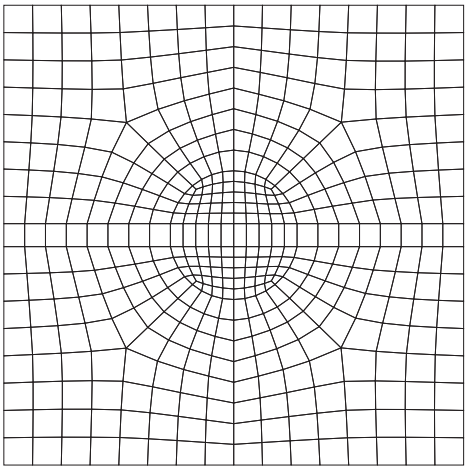

(b) Mesh configuration of RVE

Fig. 10. Mesh configurations of RVE and macro-domain.

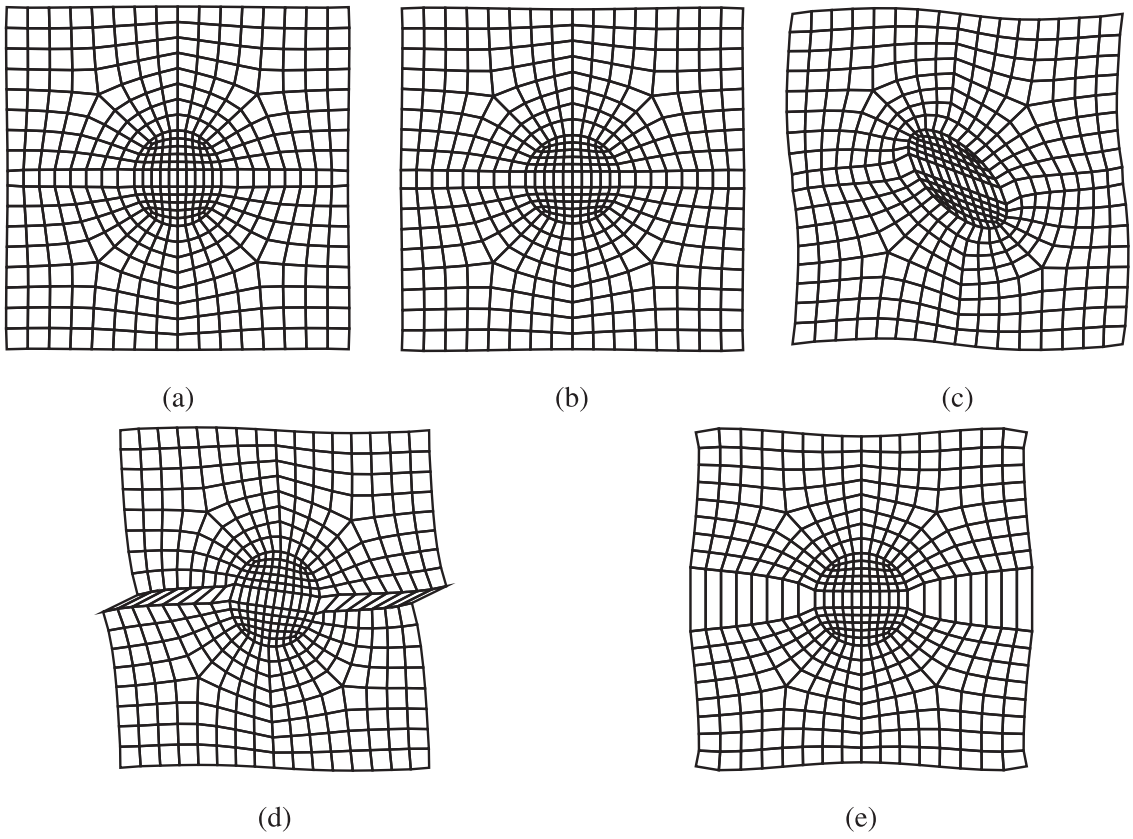

Fig. 11. Deformed configuration of RVE under unit macroscopic kinematic variables: a) $\bar{\varepsilon}_{11}=1$ b) $\bar{\varepsilon}_{22}=1$ c) $\bar{\varepsilon}_{12}=1$ d) $\beta_1=1$ e) $\beta_2=1$.

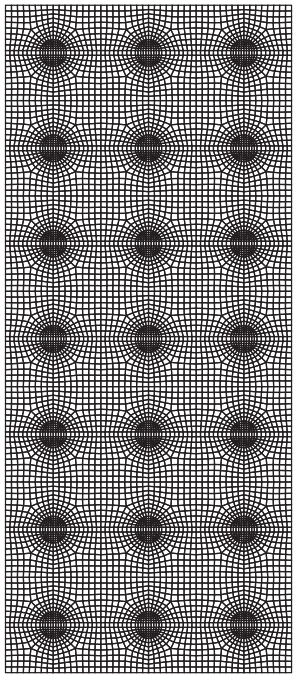

Fig. 12. Mesh configuration of the direct numerical analysis (DNA).

Substituting (51) and (52) into (49), the complementary strain field can be expressed as

$$\tilde{\varepsilon}_{ij}(\mathbf{y}) = u^h_{(i,j)}(\mathbf{y}) + F_{ik}(\mathbf{y})\bar{\alpha}^{\nabla}_{k,j} + F_{(ik,j)}\left(\bar{\alpha}_k + \bar{\alpha}^{\nabla}_{k,l}y_l\right) \tag{53}$$

where the symmetric property of F_{ik} is used to replace $F_{ik}(\mathbf{y})\bar{\alpha}^{\nabla}_{(k,j)}$ with $F_{ik}(\mathbf{y})\bar{\alpha}^{\nabla}_{k,j}$. Comparing (53) with (10), the enhanced strain and the strain fields due to the micro fluctuations are derived as

$$\tilde{\varepsilon}_{ij}(\mathbf{y}) = u^1_{(i,j)}(\mathbf{y}) + \varepsilon^*_{ij}(\mathbf{y}) \tag{54a}$$

$$\varepsilon^*_{ij}(\mathbf{y}) = F_{ik}(\mathbf{y})\bar{\alpha}^{\nabla}_{k,j} + F_{(ik,j)}\left(\bar{\alpha}_k + \bar{\alpha}^{\nabla}_{k,l}y_l\right) \tag{54b}$$

$$u^1_{(i,j)}(\mathbf{y}) = u^h_{(i,j)}(\mathbf{y}) \tag{54c}$$

where $\bar{\alpha}_k$ and $\bar{\alpha}^{\nabla}_{k,j}$, now called the enhanced tip enriched strain, should be distinguished from the enhanced strain in H-EMSHM.

Remark 8. The complementary displacement field in Eq. (46) can be considered as a useful approximation with an appropriate enrichment function (48). Generally, it is possible to use other tensors with different ranks instead of F_{ik} in (46) to approximate other specific displacement/strain fields.

6.2. Enhanced stress and macroscopic virtual power density in T-EMSHM

After extraction of the enhanced tip enriched strain, the enhanced macroscopic virtual power density, $\delta p^{\star}$, is obtained as

$$\delta p^* = \tau_k \delta\bar{\alpha}_k + \tau^{\nabla}_{kj}\delta\bar{\alpha}^{\nabla}_{k,j} \tag{55}$$

where τ_k and τ^{∇}_{kj} are the work conjugates of the enhanced tip enriched strain $\bar{\alpha}_k$ and $\bar{\alpha}^{\nabla}_{k,j}$, respectively

$$\tau_k = \frac{1}{|\Omega_\Theta|}\int_{\Omega_\Theta}\sigma_{ij}F_{(ik,j)}d\Omega \tag{56a}$$

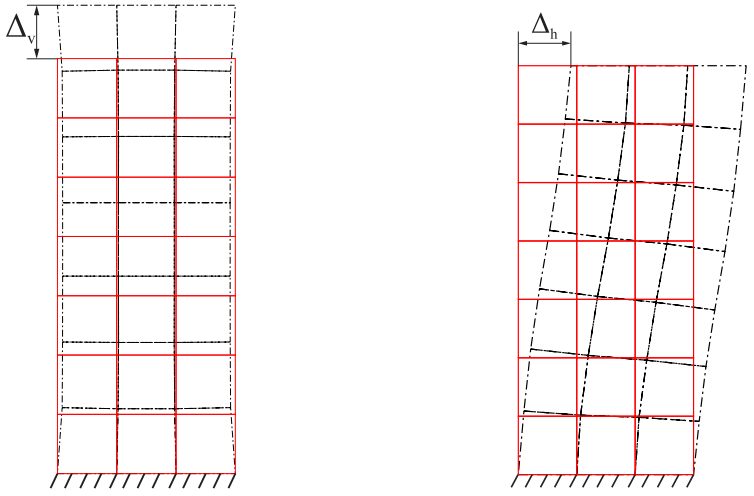

(a) Type A boundary condition (b) Type B boundary condition

Fig. 13. Horizontal and vertical prescribed displacements on the reinforced plate.

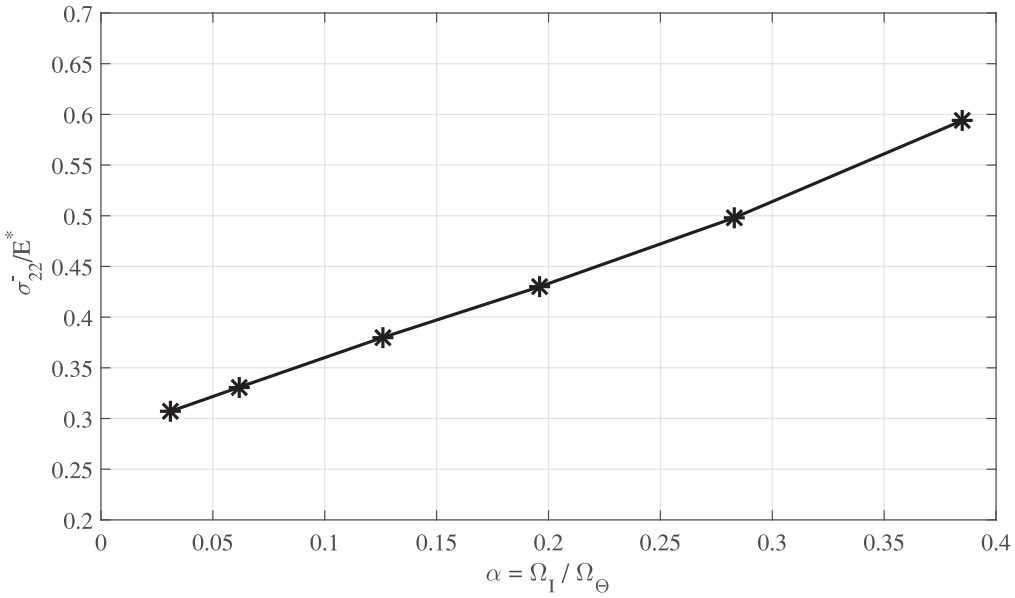

Fig. 14. Effect of volume fraction $\alpha = \frac{|\Omega_I|}{|\Omega_\Theta|}$ on the average resultant force in the 2D plate under prescribed displacement. ($\bar{\sigma}_{22} = \frac{\int_{\Gamma^{top}} \sigma_{22}(\mathbf{x})d\Gamma}{W}$ and $E^* = \sqrt{E_I E_m}$).

$$\tau_{kj}^{\nabla} = \frac{1}{|\Omega_\Theta|}\int_{\Omega_\Theta}\left(\sigma_{ij}F_{ik} + \sigma_{im}F_{(ik,m)}y_j\right)d\Omega \tag{56b}$$

Equations (55) and (56) are obtained by substituting (54b) into (15b) as

$$\begin{aligned}
\delta p^* &= \frac{1}{|\Omega_\Theta|}\int_{\Omega_\Theta}\delta\varepsilon_{ij}^*\sigma_{ij}d\Omega \\
&= \frac{1}{|\Omega_\Theta|}\int_{\Omega_\Theta}\sigma_{ij}\delta\left(F_{ik}(\mathbf{y})\bar{\alpha}_{k,j}^{\nabla} + F_{(ik,j)}\left(\bar{\alpha}_k + \bar{\alpha}_{k,l}^{\nabla}y_l\right)\right)d\Omega \\
&= \frac{1}{|\Omega_\Theta|}\int_{\Omega_\Theta}\sigma_{ij}F_{(ik,j)}\delta\bar{\alpha}_k d\Omega \\
&\quad + \frac{1}{|\Omega_\Theta|}\int_{\Omega_\Theta}\underbrace{\sigma_{ij}\left(F_{ik}\delta\bar{\alpha}_{k,j}^{\nabla} + F_{(ik,j)}\delta\bar{\alpha}_{k,l}^{\nabla}y_l\right)}_{\left(\sigma_{ij}F_{ik}+\sigma_{im}F_{(ik,m)}y_j\right)\delta\bar{\alpha}_{k,j}^{\nabla}}d\Omega
\end{aligned}$$

$$\begin{aligned}
&\times \underbrace{\left(\frac{1}{|\Omega_\Theta|}\int_{\Omega_\Theta}\sigma_{ij}F_{(ik,j)}d\Omega\right)}_{\tau_k}\delta\bar{\alpha}_k \\
&+ \underbrace{\left(\frac{1}{|\Omega_\Theta|}\int_{\Omega_\Theta}\left(\sigma_{ij}F_{ik} + \sigma_{im}F_{(ik,m)}y_j\right)d\Omega\right)}_{\tau_{kj}^{\nabla}}\delta\bar{\alpha}_{k,j}^{\nabla} \\
&\Rightarrow \delta p^* = \tau_k\delta\bar{\alpha}_k + \tau_{kj}^{\nabla}\delta\bar{\alpha}_{k,j}^{\nabla}
\end{aligned} \tag{57}$$

where the term $\sigma_{ij}F_{(ik,j)}\delta\bar{\alpha}_{k,l}^{\nabla}y_l$ in the second line of (57) has been replaced with $\sigma_{im}F_{(ik,m)}y_j\delta\bar{\alpha}_{k,j}^{\nabla}$ according to

$$\begin{aligned}
&\sigma_{ij}F_{(ik,j)}\delta\bar{\alpha}_{k,l}^{\nabla}y_l = \sigma_{im}F_{(ik,m)}\delta\bar{\alpha}_{k,s}^{\nabla}y_s = \sigma_{im}F_{(ik,m)}\delta\bar{\alpha}_{k,j}^{\nabla}y_j \\
&\Rightarrow \sigma_{ij}F_{(ik,j)}\delta\bar{\alpha}_{k,l}^{\nabla}y_l = \sigma_{im}F_{(ik,m)}\delta\bar{\alpha}_{k,j}^{\nabla}y_j
\end{aligned} \tag{58}$$

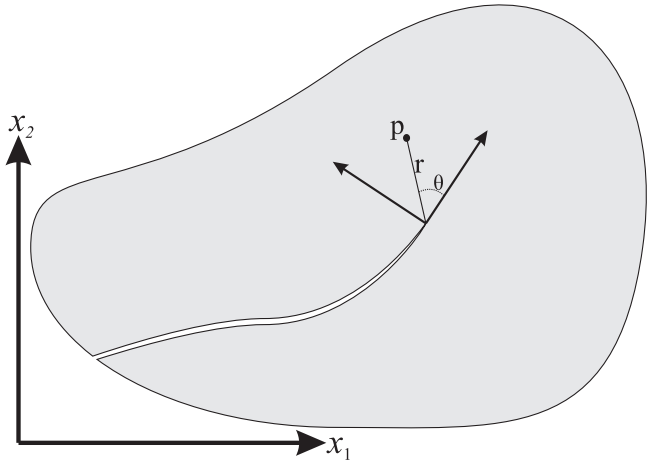

Fig. 15. Local polar coordinate system for the crack tip enrichment.

6.3. Microscopic governing equation and boundary conditions for T-EMSHM

Analogous to H-EMSHM formulation in Section 5.3, the microscopic governing equation is obtained using Eqs. (19) and (20) as

$$\int_{\Omega_\Theta} w^1_{i,j}\sigma_{ij}d\Omega = 0 \qquad \forall w_i \in \mathbf{W}^1 \tag{59}$$

with the constraint based on Eq. (60)

$$\int_{\partial\Theta} u^1_i\sigma_{ij}n_j d\Gamma = 0 \tag{60}$$

6.4. Macroscopic governing equation for T-EMSHM

Employing the same approach as H-EMSHM in Section 5.4, the macroscopic governing equations are expressed with the aid of the virtual power principle.

6.4.1. Virtual internal power

Substituting (55) and (15a) into (12), the macroscopic virtual power density is expressed by,

$$\delta p^M\left(\bar{\varepsilon}_{ij}, \varepsilon^*_{ij}\right) = \delta\bar{p}\left(\bar{\varepsilon}_{ij}\right) + \delta p^*\left(\varepsilon^*_{ij}\right) = \bar{\sigma}_{ij}\delta\bar{\varepsilon}_{ij} + \tau_k\delta\bar{\alpha}_k + \tau^\nabla_{kj}\delta\bar{\alpha}^\nabla_{k,j} \tag{61}$$

Integrating the macroscopic virtual power density of the macro-homogeneous material, equation (61), over Ω, the virtual internal power of T-EMSHM is

$$\delta P_{\text{int}} = \int_\Omega \delta p^M d\Omega = \int_\Omega \left(\bar{\sigma}_{ij}\delta\bar{\varepsilon}_{ij} + \tau_k\delta\bar{\alpha}_k + \tau^\nabla_{kj}\delta\bar{\alpha}^\nabla_{k,j}\right)d\Omega \tag{62}$$

6.4.2. Virtual external power for T-EMSHM

The virtual external power of surface force acting on Γ_t can be expressed with

$$\delta P_{ext} = \int_{\Gamma_t} t_i\delta\bar{u}_i d\Gamma \tag{63}$$

where t_i is the traction on the surface and $\bar{u}_{(i,j)} = \bar{\varepsilon}_{ij}$.

6.4.3. Principle of virtual work and macroscopic governing equation in T-EMSHM

According to the principle of virtual work, the virtual internal and external works are equal for any independent virtual $\delta\bar{u}_i$ and $\delta\bar{\alpha}_i$. Substituting (62) and (63) into (43), the weak form of the macroscopic governing equation can be written as

$$\int_\Omega \left(\bar{\sigma}_{ij}\delta\bar{\varepsilon}_{ij} + \tau_k\delta\bar{\alpha}_k + \tau^\nabla_{kj}\delta\bar{\alpha}^\nabla_{k,j}\right)d\Omega - \int_{\Gamma_t} t_i\delta\bar{u}_i d\Gamma = 0 \tag{64a}$$

$$\bar{u}_i(\mathbf{x}) = \bar{u}^d_i \qquad \mathbf{x} \in \Gamma_D \tag{64b}$$

where (64a) is true for any variation of $\delta\bar{u}_i$ and $\delta\bar{\alpha}_k$, and $\bar{u}^d_i$ in (64b) is the prescribed displacement on Γ_D.

Remark 9. It is possible to combine both Heaviside H-EMSHM and tip T-EMSHM enrichments in the micro-based framework, if investigation of crack singularity within the RVE is in hand.

Remark 10. It should be noted that the enrichment function $\sqrt{r}\sin\left(\frac{\theta}{2}\right)$ (introduced in Eq. (48)) is also discontinuous on crack surface due to the characteristic of $\sin\left(\frac{\theta}{2}\right)$ (Bayesteh et al., 2015). Consequently, the tip enrichment function (48) is discontinuous across crack faces and does not require an independent Heaviside enrichment within an element. As a result, the tip enrichment can be used for cases where crack tip is located anywhere inside the RVE. For any complicated crack path in the RVE, however, H-EMSHM and T-EMSHM should be simultaneously adopted.

6.5. Numerical example of T-EMSHM

The aim of T-EMSHM is to consider severe strain gradient problems, in which the first order homogenization methods fail to perform, by taking a priori known appropriate basis functions into the formulation. To evaluate the formulation, a cracked plate under uniform prescribed tension is considered, as depicted in Fig. 16. Geometric specifications and mechanical properties are:

$H = 12 \quad (mm)$ $\qquad W = 10 \quad (mm)$ $\qquad a = 4 \quad (mm)$

$\bar{\sigma} = 50 \quad (MPa)$ $\qquad E_m = 68.9 \quad (GPa)$ $\qquad E_I = 379.2 \quad (GPa)$

$\nu_m = 0.33$ $\qquad \nu_I = 0.22$ $\qquad \frac{\Omega_I}{\Omega_\Theta} = 0.267$

As a reference benchmark, a very fine finite element mesh (Fig. 17) including 140160 four node ("Q4") elements (140629 nodes) is employed to model all details. Furthermore, a macro homogeneous model with 30 Q4 elements (42 nodes) in parallel with the RVE model, with 1168 Q4 elements (1205 nodes), are used to evaluate T-EMSHM. Additionally, the first order homogenization method, with the same macro/RVE mesh as T-EMSHM, is considered for comparison. The homogeneous macro and RVE mesh configurations are shown in Fig. 18. The crack is explicitly meshed in the macroscopic scale, however, a general crack-independent XFEM mesh can also be adopted. The proposed T-EMSHM is employed to consider singular distribution of strain field in a local region around an existing macroscopic crack. Consequently, only the elements around the crack tip are enriched in this example. It is generally possible to enrich farther elements, but it is not recommended due to the characteristic of singular function $\frac{1}{\sqrt{r}}$, that vanishes rapidly.

Due to the fact that the enrichment function (48) varies with respect to the crack tip location, the corresponding basic modes do not remain unique for all RVEs and depend on the location of RVE. In Fig. 19, two basic modes associated with the additional macroscopic kinematic variable in T-EMSHM are shown for the RVE located at nearest gauss point to the macroscopic crack tip.

The von Mises stress contours on an RVE near the crack tip, as depicted in Fig. 16, are compared in Fig. 20 for the reference (direct modeling), T-EMSHM and first order homogenization solutions. It is clearly observed that T-EMSHM is more accurate than the first order homogenization from both the magnitude and spatial distribution points of view. The first order homogenization method shows almost a uniform stress distribution in Fig. 20c because of its underlying constant macro stress assumption, while the enrichment introduced in (48) is capable of reproducing the singular and non-constant macro stress field in T-EMSHM, as depicted

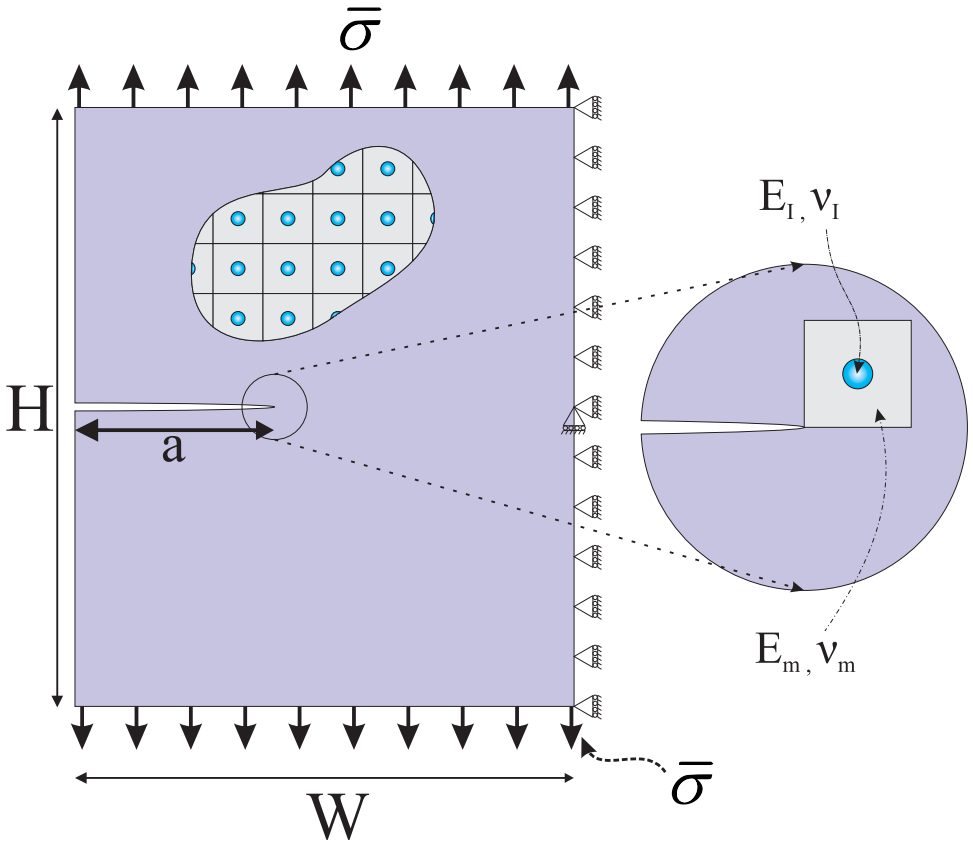

Fig. 16. Rectangular cracked plate under tension.

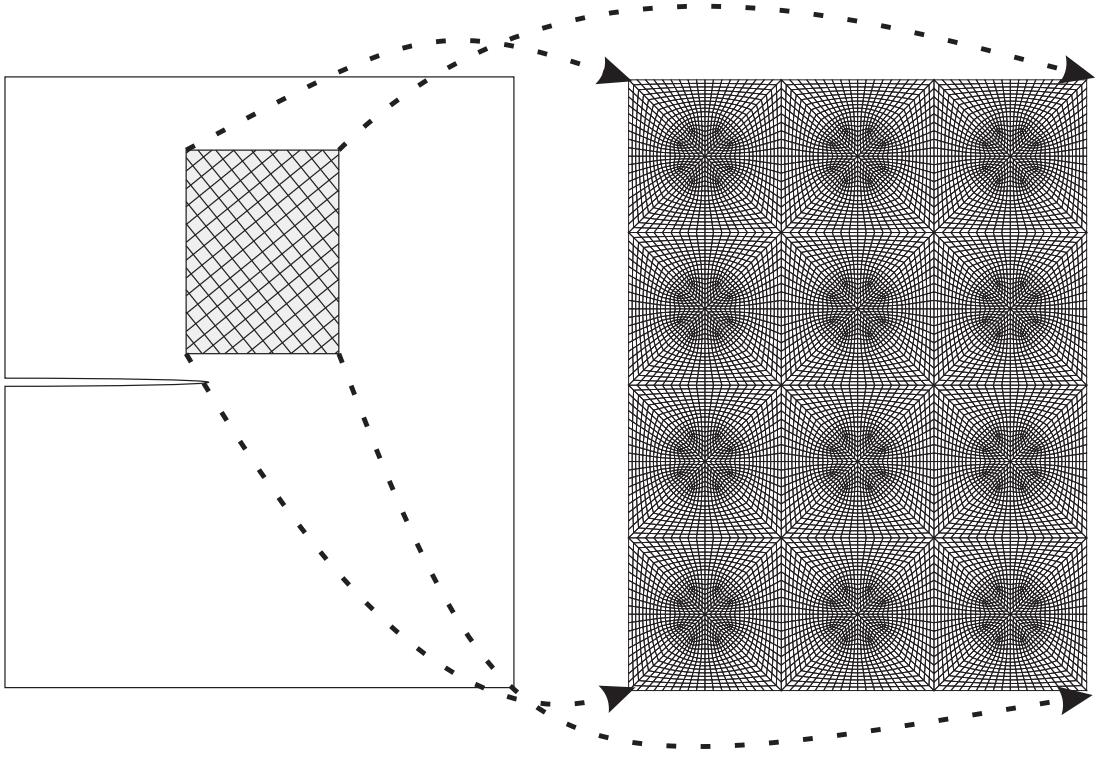

Fig. 17. Mesh configuration of the direct numerical modeling of cracked rectangular plate.

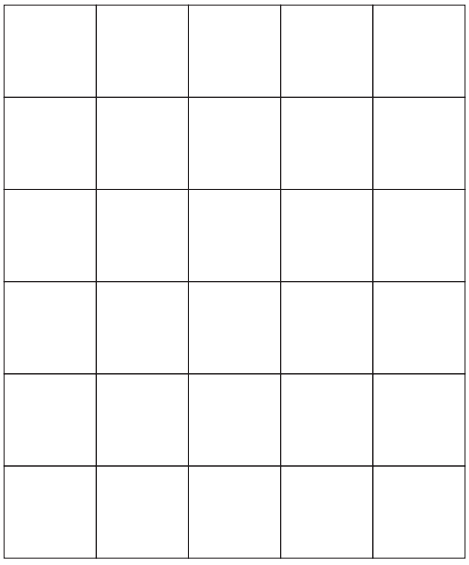

(a) Mesh configuration for the macroscopic homogeneous domain.

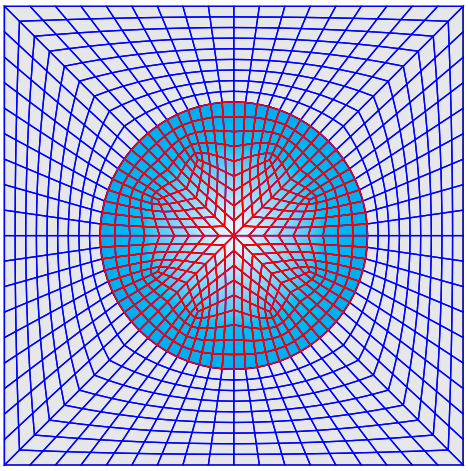

(b) Mesh configuration for the RVE.

Fig. 18. Mesh configurations of homogeneous macro-domain and RVE.

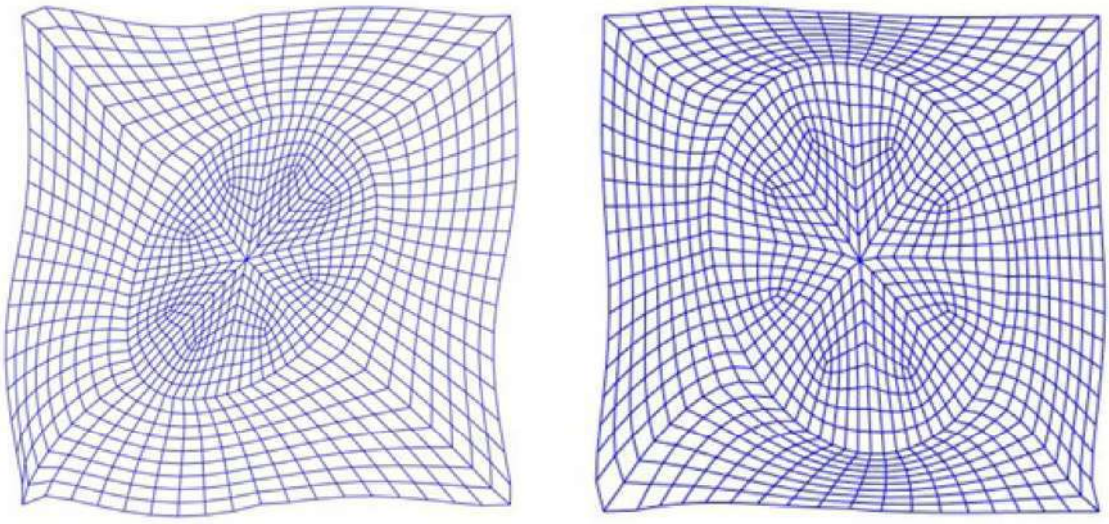

(a) $\bar{\alpha}_1 = 1 \quad and \quad \bar{\alpha}_2 = 0$ (b) $\bar{\alpha}_1 = 0 \quad and \quad \bar{\alpha}_2 = 1$

Fig. 19. Deformed configuration (microflactuation) of RVE under unit macroscopic T-EMSHM kinematic variable.

Table 4
Comparison of maximum von Mises stress and the corresponding error for T-EMSHM and the first order homogenization. ($error\% = \frac{\sigma_{VM}^{ref} - \sigma_{VM}}{\sigma_{VM}^{ref}} \times 100$).

Method	Maximum von Mises stress (MPa)	error (%)
reference (DNA)	509.5	–
T-EMSHM	467.7	8
first order homogenization	123.5	75

in Fig. 20b. The maximum values of von Mises stress for direct, T-EMSHM and first order methods are 509.5, 467.7 and 123.5 *MPa*, respectively. The error of T-EMSHM and first order homogenization methods are reported in Table 4, which shows a major improvement by T-EMSHM.

7. Conclusion

The main focus of this paper has been to discuss development of the general framework of new kinematic variables to overcome the shortcomings of conventional homogenization problems. According to the concepts of homogenization, additional kinematic variables can either be macro-based or micro-based. The micro-based approach has been proposed and particularly explored in this study as a versatile tool to derive appropriate additional variables based on the existing phenomena in RVE. Another words, the new variables are derived from the microscopic concepts rather than the macroscopic one. This new approach is suitable for handling the drawbacks of conventional homogenization methods.

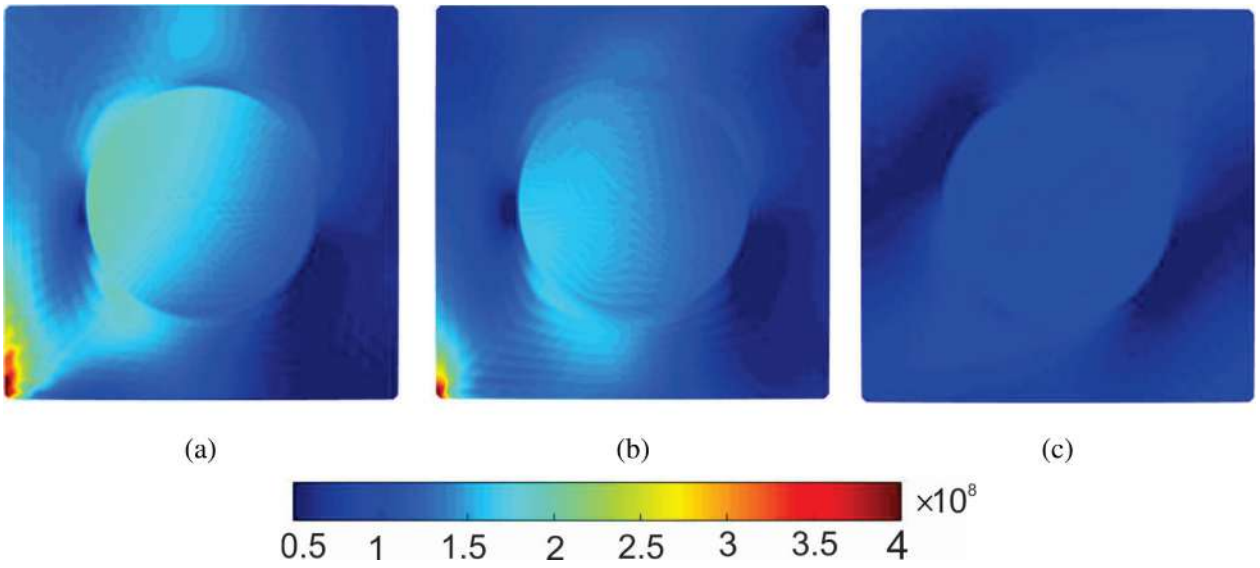

Fig. 20. Von Mises stress contour: a) reference direct solution b) T-EMSHM c) first order homogenization.

Accordingly, a general formulation based on the micro-based framework, entitled the enriched multiscale homogenization method (EMSHM), has been developed using the Hill-Mandel theory to extract the work conjugate of new variables. EMSHM has then been employed to formulate governing macroscopic equation to study a cracked RVE and a problem with severe strain gradient near a macro crack tip. First, the Heaviside enriched multiscale homogenization method (H-EMSHM) has been developed based on the XFEM formulation in the RVE to incorporate the effects of microscopic cracking on macroscopic formulation. H-EMSHM has successfully been evaluated with basic examples.

Furthermore, the crack tip enriched multiscale homogenization method (T-EMSHM) has been established based on the inspiration from the crack tip enrichment of the extended numerical method with the intention of considering severe macro strain gradient on the RVE. The existing tip enrichment has been used to extract new kinematic variables according to the EMSHM. Numerical simulation of a cracked plate showed the superior performance of T-EMSHM from both the spatial distribution and magnitude of stress around the crack tip. It should be emphasized that, apart from the present application in a near crack tip domain, this formulation can be well utilized in different extreme problems with proper adoption of appropriate enrichment functions. Mixed mode fracture, crack propagation and considering general softening cases are among the ongoing research works.

Acknowledgements

The authors wish to gratefully acknowledge the technical support of the High Performance Computing Lab, School of Civil Engineering, University of Tehran.

The financial support of Iran National Science Foundation (INSF) is gratefully acknowledged.

Appendix A. First order multiscale homogenization

Substituting Eqs. (1) into (2) results in

$$\begin{aligned}\delta\bar{p}\left(\bar{\varepsilon}_{ij}(\mathbf{x})\right) &= \frac{1}{|\Omega_\Theta|}\int_{\Omega_\Theta}\sigma_{ij}(\mathbf{x},\mathbf{y})\delta\left(\bar{\varepsilon}_{ij}(\mathbf{x})+\tilde{\varepsilon}_{ij}(\mathbf{y})\right)d\Omega\\ &= \frac{1}{|\Omega_\Theta|}\int_{\Omega_\Theta}\sigma_{ij}(\mathbf{x},\mathbf{y})\delta\bar{\varepsilon}_{ij}(\mathbf{x})d\Omega\\ &\quad+\frac{1}{|\Omega_\Theta|}\int_{\Omega_\Theta}\sigma_{ij}(\mathbf{x},\mathbf{y})\delta\tilde{\varepsilon}_{ij}(\mathbf{y})d\Omega\\ &= \underbrace{\left(\frac{1}{|\Omega_\Theta|}\int_{\Omega_\Theta}\sigma_{ij}(\mathbf{x},\mathbf{y})d\Omega\right)}_{\bar{\sigma}_{ij}(\mathbf{x})}\delta\bar{\varepsilon}_{ij}(\mathbf{x})\\ &\quad+\frac{1}{|\Omega_\Theta|}\int_{\Omega_\Theta}\sigma_{ij}(\mathbf{x},\mathbf{y})\delta\tilde{\varepsilon}_{ij}(\mathbf{y})d\Omega\end{aligned} \tag{A.1}$$

$$\begin{aligned}&\Rightarrow \delta\bar{p}\left(\bar{\varepsilon}_{ij}(\mathbf{x})\right) = \bar{\sigma}_{ij}(\mathbf{x})\delta\bar{\varepsilon}_{ij}(\mathbf{x})+\frac{1}{|\Omega_\Theta|}\int_{\Omega_\Theta}\sigma_{ij}(\mathbf{x},\mathbf{y})\delta\tilde{\varepsilon}_{ij}(\mathbf{y})d\Omega\\ &\Rightarrow \left[\delta\bar{p}\left(\bar{\varepsilon}_{ij}(\mathbf{x})\right)-\bar{\sigma}_{ij}(\mathbf{x})\delta\bar{\varepsilon}_{ij}(\mathbf{x})\right]-\frac{1}{|\Omega_\Theta|}\int_{\Omega_\Theta}\sigma_{ij}(\mathbf{x},\mathbf{y})\delta\tilde{\varepsilon}_{ij}(\mathbf{y})d\Omega=0\end{aligned} \tag{A.2}$$

Knowing that $\delta\bar{p}\left(\bar{\varepsilon}_{ij}(\mathbf{x})\right)$ depends on $\bar{\varepsilon}_{ij}$, and $\delta\bar{\varepsilon}_{ij}$ and $\delta\tilde{\varepsilon}_{ij}$ are arbitrary, the virtual macroscopic power density

$$\begin{aligned}&\delta\bar{p}\left(\bar{\varepsilon}_{ij}(\mathbf{x})\right)-\bar{\sigma}_{ij}(\mathbf{x})\delta\bar{\varepsilon}_{ij}(\mathbf{x})=0\\ &\Rightarrow \delta\bar{p}(\mathbf{x})=\bar{\sigma}_{ij}(\mathbf{x})\delta\bar{\varepsilon}_{ij}(\mathbf{x})\end{aligned} \tag{A.3}$$

is derived by setting $\delta\tilde{\varepsilon}_{ij}(\mathbf{y})=0$ and $\delta\bar{\varepsilon}_{ij}(\mathbf{x})$ is arbitrary, where

$$\bar{\sigma}_{ij}(\mathbf{x}) = \frac{1}{|\Omega_\Theta|}\int_{\Omega_\Theta}\sigma_{ij}(\mathbf{x},\mathbf{y})d\Omega \tag{A.4}$$

Eq. (A.3) demonstrates that $\bar{\sigma}_{ij}(\mathbf{x})$ is the work conjugate of the virtual macroscopic strain $\delta\bar{\varepsilon}_{ij}(\mathbf{x})$ in the virtual macroscopic density function and (A.4) shows that the macroscopic stress $\bar{\sigma}_{ij}(\mathbf{x})$ is the average of stress on RVE. The governing equation in RVE is then achieved by setting $\delta\bar{\varepsilon}_{ij}(\mathbf{x})=0$ in (A.2)

$$\int_{\Omega_\Theta}\sigma_{ij}(\mathbf{x},\mathbf{y})\delta\tilde{\varepsilon}_{ij}(\mathbf{y})d\Omega=0 \tag{A.5}$$

The boundary condition of the above equation is applied according to constraint (5). It is proved that with the periodic boundary conditions on the opposite sides of RVE, (5) holds automatically.

Appendix B. Boundary conditions of RVE

In order to guarantee Eq. (20), appropriate essential/natural boundary conditions should be selected. The unknown traction

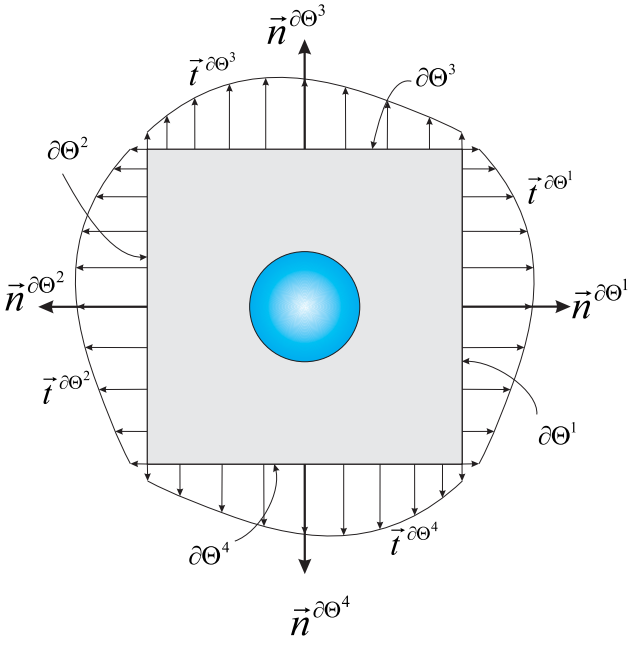

Fig. B.21. Unit normal vectors on the boundary of RVE. $\vec{n}^{\partial\Theta^k} = n_i^{\partial\Theta^k}$ and $\vec{t}^{\partial\Theta^k} = t_i^{\partial\Theta^k}$ are n_i and t_i on the surface $\partial\Theta^k$, respectively.

field t_i on $\partial\Theta$ is defined using the unknown stress tensor$\lambda_{ij}(\mathbf{y})$ with $t_i = \lambda_{ij} n_j$. λ_{ij} is calculated in a way that (20) is held automatically. Hence, the equilibrium equation on the RVE can be expressed as

$$\sigma_{ij,j}(\mathbf{y}) = 0 \qquad \mathbf{y} \in \Omega_\Theta \tag{B.1a}$$

$$\sigma_{ij}(\mathbf{y}) n_j = \lambda_{ij} n_j \qquad \mathbf{y} \in \partial\Theta = \bigcup_{k=1}^{4} \partial\Theta^k \tag{B.1b}$$

$$\int_{\partial\Theta} u_i^1 \lambda_{ij} n_j d\Gamma = 0 \tag{B.1c}$$

n_j is the unit normal vector to the boundary, as depicted in Fig. B.21. (B.1c) represents the constraint (20) and (B.1b) is the natural boundary condition in terms of $\lambda_{ij}(\mathbf{y})$.

The weak form of equations (B.1) is expressed with

$$-\int_{\Omega_\Theta} w_{i,j}^1 \sigma_{ij} d\Omega + \int_{\partial\Theta} w_i^1 \lambda_{ij} n_j d\Gamma + \int_{\partial\Theta} u_i^1 \delta\lambda_{ij} n_j d\Gamma = 0$$
$$(\forall w_i^1 \in V_{W^1} \;\&\; \forall \delta\lambda_{ij} \in V_\lambda) \tag{B.2}$$

or equivalently,

$$-\int_{\Omega_\Theta} w_{i,j}^1 \sigma_{ij} d\Omega + \int_{\partial\Theta} w_i^1 \lambda_{ij} n_j d\Gamma = 0 \qquad \forall w_i^1 \in V_{W^1} \tag{B.3a}$$

$$\int_{\partial\Theta} u_i^1 \delta\lambda_{ij} n_j d\Gamma = 0 \qquad \forall \delta\lambda_{ij} \in V_\lambda \tag{B.3b}$$

where V_{W^1} and V_{λ^1} are the space of all admissible functions of w_i^1 and $\delta\lambda_{ij}$, respectively. Different types of boundary conditions can be achieved based on the space of V_λ in (B.3b):

1. *Constant stress:* If V_λ includes only constant functions, (B.3b) is simplified to

$$\delta\lambda_{ij} \int_{\partial\Theta} u_i^1 n_j d\Gamma = 0 \Rightarrow \int_{\partial\Theta} u_i^1 n_j d\Gamma = 0 \tag{B.4}$$

(B.4) is the minimal kinematic boundary condition.

2. *Periodic stress:* If V_λ includes all admissible periodic functions defined with

$$V_\lambda = \left\{ \lambda_{ij}(\mathbf{y}) \text{ defined in } \Omega_\Theta \,\middle|\, \lambda_{ij}(\mathbf{y}),\ \mathbf{Y}-\text{periodic and smooth enough} \right\} \tag{B.5}$$

(B.3b) is reduced to

$$\begin{aligned}
&\int_{\partial\Theta=\partial\Theta^1\cup\partial\Theta^2\cup\partial\Theta^3\cup\partial\Theta^4} u_i^1 \delta\lambda_{ij} n_j d\Gamma = 0 \\
&\Rightarrow \int_{\partial\Theta^1} u_i^1\left(\mathbf{y}^{\partial\Theta^1}\right)\delta\lambda_{ij}\left(\mathbf{y}^{\partial\Theta^1}\right) n_i^{\partial\Theta^1} d\Gamma \\
&\quad + \int_{\partial\Theta^2} u_i^1\left(\mathbf{y}^{\partial\Theta^2}\right)\delta\lambda_{ij}\left(\mathbf{y}^{\partial\Theta^2}\right) n_i^{\partial\Theta^2} d\Gamma \\
&\quad + \int_{\partial\Theta^3} u_i^1\left(\mathbf{y}^{\partial\Theta^3}\right)\delta\lambda_{ij}\left(\mathbf{y}^{\partial\Theta^3}\right) n_i^{\partial\Theta^3} d\Gamma \\
&\quad + \int_{\partial\Theta^4} u_i^1\left(\mathbf{y}^{\partial\Theta^4}\right)\delta\lambda_{ij}\left(\mathbf{y}^{\partial\Theta^4}\right) n_i^{\partial\Theta^4} d\Gamma = 0
\end{aligned} \tag{B.6}$$

where $\mathbf{y}^{\partial\Theta^k} \in \partial\Theta^k$ and $n_i^{\partial\Theta^k}$ are depicted in Figure B.21. Defining $\mathbf{Y}_h$ and $\mathbf{Y}_v$

$$\mathbf{y}^{\partial\Theta^2} = \mathbf{y}^{\partial\Theta^1} + \mathbf{Y}_h \tag{B.7a}$$

$$\mathbf{y}^{\partial\Theta^4} = \mathbf{y}^{\partial\Theta^3} + \mathbf{Y}_v \tag{B.7b}$$

and using

$$\delta\lambda_{ij}\left(\mathbf{y}^{\partial\Theta^1}\right) = \delta\lambda_{ij}\left(\mathbf{y}^{\partial\Theta^2}\right) \tag{B.8a}$$

$$\delta\lambda_{ij}\left(\mathbf{y}^{\partial\Theta^3}\right) = \delta\lambda_{ij}\left(\mathbf{y}^{\partial\Theta^4}\right) \tag{B.8b}$$

Eq. (B.6) can be rearranged due to the periodicity of λ_{ij},

$$\begin{aligned}
&\int_{\partial\Theta^1} \delta\lambda_{ij}\left(\mathbf{y}^{\partial\Theta^1}\right)\left[u_i^1\left(\mathbf{y}^{\partial\Theta^1}\right) - u_i^1\left(\mathbf{y}^{\partial\Theta^1} + \mathbf{Y}_h\right)\right] n_i^{\partial\Theta^1} d\Gamma \\
&\quad + \int_{\partial\Theta^3} \delta\lambda_{ij}\left(\mathbf{y}^{\partial\Theta^3}\right)\left[u_i^1\left(\mathbf{y}^{\partial\Theta^3}\right) - u_i^1\left(\mathbf{y}^{\partial\Theta^3} + \mathbf{Y}_v\right)\right] n_i^{\partial\Theta^3} d\Gamma = 0
\end{aligned} \tag{B.9}$$

Having employed functional principals, the final periodic displacement on $u_i^1(\mathbf{y})$ are derived as

$$u_i^1\left(\mathbf{y}^{\partial\Theta^1}\right) - u_i^1\left(\mathbf{y}^{\partial\Theta^1} + \mathbf{Y}_h\right) = 0 \Rightarrow u_i^1\left(\mathbf{y}^{\partial\Theta^1}\right) = u_i^1\left(\mathbf{y}^{\partial\Theta^2}\right) \tag{B.10a}$$

$$u_i^1\left(\mathbf{y}^{\partial\Theta^3}\right) - u_i^1\left(\mathbf{y}^{\partial\Theta^3} + \mathbf{Y}_v\right) = 0 \Rightarrow u_i^1\left(\mathbf{y}^{\partial\Theta^3}\right) = u_i^1\left(\mathbf{y}^{\partial\Theta^4}\right) \tag{B.10b}$$

3. *Homogeneous boundary condition:* if V_λ encompasses all admissible functions on Γ_Θ, (B.3b) results in

$$u_i^1(\mathbf{y}) n_j = 0 \qquad \mathbf{y} \in \partial\Theta \tag{B.11}$$

Appendix C. XFEM displacement field

Defining a new enriched DOF $\check{a}_i^k$

$$\hat{a}_i^k = \beta_i + \check{a}_i^k \tag{C.1}$$

and substituting (C.1) into equation (21), relation (C.2) is obtained as

$$\begin{aligned}\tilde{u}_i(\mathbf{y}) &= \sum_{k=1}^{n_{stn}} N_k \hat{u}_i^k + \sum_{k=1}^{n_{en}} N_k [H(\xi(\mathbf{y})) - H(\xi(\mathbf{y}_k))]\left(\beta_i + \breve{a}_i^k\right) \\ &= \sum_{k=1}^{n_{stn}} N_k \hat{u}_i^k + \sum_{k=1}^{n_{en}} N_k [H(\xi(\mathbf{y})) - H(\xi(\mathbf{y}_k))]\beta_i \\ &\quad + \sum_{k=1}^{n_{en}} N_k [H(\xi(\mathbf{y})) - H(\xi(\mathbf{y}_k))]\breve{a}_i^k \\ &= \sum_{k=1}^{n_{stn}} N_k \hat{u}_i^k + \underbrace{\left(\sum_{k=1}^{n_{en}} N_k\right)}_{=1} H(\xi(\mathbf{y}))\beta_i - \underbrace{\left(\sum_{k=1}^{n_{en}} N_k H(\xi(\mathbf{y}_k))\right)}_{=\sum_{k=\{n_{en}^+\}} N_k} \beta_i \\ &\quad + \sum_{k=1}^{n_{en}} N_k [H(\xi(\mathbf{y})) - H(\xi(\mathbf{y}_k))]\breve{a}_i^k \\ &= \sum_{k=1}^{n_{stn}} N_k \hat{u}_i^k + \left(H(\xi(\mathbf{y})) - \sum_{k=\{n_{en}^+\}} N_k\right)\beta_i \\ &\quad + \sum_{k=1}^{n_{en}} N_k [H(\xi(\mathbf{y})) - H(\xi(\mathbf{y}_k))]\breve{a}_i^k \end{aligned} \tag{C.2}$$

where $\{n_{en}^+\}$ is the set of nodes in which $H(\xi(\mathbf{y}_k)) > 0$, and $\xi(\mathbf{y})$ has been defined in (23). The final form of this equation is expressed as,

$$\begin{aligned}\tilde{u}_i(\mathbf{y}) &= (H(\xi(\mathbf{y})) - \varphi(\mathbf{y}))\beta_i + \sum_{k=1}^{n_{stn}} N_k \hat{u}_i^k \\ &\quad + \sum_{k=1}^{n_{en}} N_k [H(\xi(\mathbf{y})) - H(\xi(\mathbf{y}_k))]\breve{a}_i^k \end{aligned} \tag{C.3}$$

where

$$\varphi(\mathbf{y}) = \sum_{k=\{n_{en}^+\}} N_k \tag{C.4}$$

or in the simple form of

$$\tilde{u}_i(\mathbf{y}) = u_i^*(\mathbf{y}) + u_i^1(\mathbf{y}) \tag{C.5}$$

where

$$u_i^*(\mathbf{y}) = (H(\xi(\mathbf{y})) - \varphi(\mathbf{y}))\beta_i \tag{C.6a}$$

$$u_i^1(\mathbf{y}) = \sum_{k=1}^{n_{stn}} N_k \hat{u}_i^k + \sum_{k=1}^{n_{en}} N_k [H(\xi(\mathbf{y})) - H(\xi(\mathbf{y}_k))]\breve{a}_i^k \tag{C.6b}$$

$H(.)$ and $\varphi(.)$ are depicted in Fig. 3. It should be emphasized that the displacement field $u_i^1(\mathbf{y})$ remains discontinuous and is solved using the XFEM discretization. It also requires additional Gauss integration points, which are provided by the sub-triangulation integration technique.

Appendix D. Derivation of equation 49

The Complementary displacement field can be expressed with (46)

$$\tilde{u}_i(\mathbf{y}) = u_i^h(\mathbf{y}) + F_{ik}\gamma_k(\mathbf{y}) \tag{D.1}$$

From the compatibility conditions of continuum mechanics, the complementary strain field is

$$\tilde{\varepsilon}_{ij} = \tilde{u}_{(i,j)} = \frac{u_{i,j} + u_{j,i}}{2} = \underbrace{\frac{u_{i,j}^h + u_{j,i}^h}{2}}_{u_{(i,j)}^h} + \underbrace{\frac{(F_{ik}\gamma_k)_{,j} + \left(F_{jk}\gamma_k\right)_{,i}}{2}}_{T} \tag{D.2}$$

Expanding the term T in (D.2)

$$\begin{aligned} T &= \frac{(F_{ik}\gamma_k)_{,j} + \left(F_{jk}\gamma_k\right)_{,i}}{2} = \frac{\left(F_{ik,j}\gamma_k + F_{ik}\gamma_{k,j}\right) + \left(F_{jk,i}\gamma_k + F_{jk}\gamma_{k,i}\right)}{2} \\ &= \underbrace{\frac{F_{ik,j}\gamma_k + F_{jk,i}\gamma_k}{2}}_{T_1} + \underbrace{\frac{F_{ik}\gamma_{k,j} + F_{jk}\gamma_{k,i}}{2}}_{T_2} \end{aligned} \tag{D.3}$$

and employing

$$T_1 = \frac{F_{ik,j}\gamma_k + F_{jk,i}\gamma_k}{2} = \underbrace{\frac{F_{ik,j} + F_{jk,i}}{2}}_{F_{(ik,j)}}\gamma_k = F_{(ik,j)}\gamma_k \tag{D.4a}$$

$$\begin{aligned} T_2 &= \frac{F_{ik}\gamma_{k,j} + F_{jk}\gamma_{k,i}}{2} = \frac{f^{enr}\delta_{ik}\gamma_{k,j} + f^{enr}\delta_{jk}\gamma_{k,i}}{2} = \frac{f^{enr}\delta_{ik}\gamma_{k,j} + f^{enr}\gamma_{j,i}}{2} \\ &= \frac{f^{enr}\delta_{ik}\gamma_{k,j} + f^{enr}\delta_{ik}\gamma_{j,k}}{2} = \underbrace{f^{enr}\delta_{ik}}_{F_{ik}} \underbrace{\frac{\gamma_{k,j} + \gamma_{j,k}}{2}}_{\gamma_{(k,j)}} = F_{ik}\gamma_{(k,j)} \end{aligned} \tag{D.4b}$$

substituting (D.4a) and (D.4b) into (D.3) and using (D.2) with

$$\tilde{\varepsilon}_{ij}(\mathbf{y}) = u_{(i,j)}^h(\mathbf{y}) + F_{ik}\gamma_{(k,j)}(\mathbf{y}) + F_{(ik,j)}\gamma_k(\mathbf{y}) \tag{D.5}$$

the final relation (D.5) is obtained, which is similar to (49). It should be noted that relation (47) is used in expanding (D.4b).

Appendix E. Coupled micro-macro solution procedure

In the present formulation, the macroscopic coupled constitutive tensor is derived using the unit linear perturbation of kinematic macroscopic variables in (36) (Yuan and Fish, 2008). A typical 2D coupled constitutive matrix in 2D problem can be derived in matrix notation as

$$\begin{Bmatrix}\vec{\sigma}\\ \vec{\gamma}\end{Bmatrix} = \begin{bmatrix}[C^{\sigma-\varepsilon}] & [C^{\sigma-\beta}]\\ [C^{\gamma-\varepsilon}] & [C^{\gamma-\beta}]\end{bmatrix}\begin{Bmatrix}\vec{\varepsilon}\\ \vec{\beta}\end{Bmatrix} \tag{E.1}$$

where

$$\vec{\sigma} = \begin{Bmatrix}\sigma_{11}\\ \sigma_{22}\\ \sigma_{12}\end{Bmatrix}, \quad \vec{\varepsilon} = \begin{Bmatrix}\varepsilon_{11}\\ \varepsilon_{22}\\ 2\varepsilon_{12}\end{Bmatrix}, \quad \vec{\gamma} = \begin{Bmatrix}\gamma_1\\ \gamma_2\end{Bmatrix}, \quad \vec{\beta} = \begin{Bmatrix}\beta_1\\ \beta_2\end{Bmatrix} \tag{E.2}$$

with nonzero off-diagonal terms. Procedures of solving the coupled macro and micro equations at micro and macro levels, are presented in the following.

Solution algorithm in the RVE level

For each RVE:

- Step 1. Given the macroscopic strain $\bar{\varepsilon}_{ij}$ and the macroscopic kinematic variable β_i from macro solution, find the micro fluctuation field $u_i^1(\mathbf{y})$ from (36) and the boundary condition (37a) with the constraint (37b) on crack surface.
  Note 1: An iterative solution should be adopted for nonlinear cases in this step.
  Note 2: $\bar{\varepsilon}_{ij}$ and β_i are required for solving Eq. (36), due to the fact that σ_{ij} is a function of $\bar{\varepsilon}_{ij}$, β_i and $u_{(i,j)}^1$ (i.e. $\sigma_{ij}(\bar{\varepsilon}_{ij}, \beta_i, u_{(i,j)}^1(\mathbf{y}))$).
- Step 2. Find the macroscopic work conjugates $\bar{\sigma}_{ij}$ and γ_i from (16) and (33), respectively.
- Step 3. Compute the tangential macroscopic constitutive matrix by the unit linear perturbation of $\bar{\varepsilon}_{ij}$ and β_i in the form of Eq. (E.1).

Solution algorithm in the macroscopic level

- Step 1. Given the initial tangential constitutive matrix (presented symbolically in Eq. (E.1)), find the initial values of $\bar{\varepsilon}_{ij}$ and β_i by solving (44)
- Step 2. Given $\bar{\varepsilon}_{ij}$ and β_i from the previous step, compute $\bar{\sigma}_{ij}$ and γ_i from solution algorithm in RVE level.
- Step 3. Compute the macroscopic residual force r_i as

$$r_i = \int_\Omega \left(\bar{\sigma}_{ij}\delta\bar{\varepsilon}_{ij} + \gamma_i\delta\beta_i\right)d\Omega - \int_\Omega \left(b_i\delta\bar{u}_i + B_i\delta\beta_i\right)d\Omega - \int_{\Gamma_t} t_i\delta\bar{u}d\Gamma \tag{E.3}$$

- Step 4. check the convergence criterion: $norm(r_i) < tol$, and go to the *Step1 1* if necessary.

References

Bažant, Z.P., Jirásek, M., 2002. Nonlocal integral formulations of plasticity and damage: Survey of progress. J. Eng. Mech. 128, 1119–1149. doi:10.1061/(ASCE)0733-9399(2002)128:11(1119).

Bayesteh, H., Afshar, A., Mohammdi, S., 2015. Thermo-mechanical fracture study of inhomogeneous cracked solids by the extended isogeometric analysis method. Eur. J. Mech. - A/Solids 51, 123–139. doi:10.1016/j.euromechsol.2014.12.004. http://www.sciencedirect.com/science/article/pii/S0997753814001855.

Bayesteh, H., Mohammadi, S., 2013. {XFEM} fracture analysis of orthotropic functionally graded materials. Compos. Part B 44, 8–25. doi:10.1016/j.compositesb.2012.07.055. http://www.sciencedirect.com/science/article/pii/S1359836812005100.

Bosco, E., Kouznetsova, V.G., Coenen, E.W.C., Geers, M.G.D., Salvadori, A., 2014. A multiscale framework for localizing microstructures towards the onset of macroscopic discontinuity. Comput. Mech. 54, 299–319. doi:10.1007/s00466-014-0986-4.

Bosco, E., Kouznetsova, V.G., Geers, M.G.D., 2015. Multi-scale computational homogenization–localization for propagating discontinuities using x-fem. Int. J. Numer. Methods Eng. 102, 496–527. doi:10.1002/nme.4838.

Coenen, E., Kouznetsova, V., Geers, M., 2012. Multi-scale continuous–discontinuous framework for computational-homogenization–localization. J. Mech. Phys. Solids 60, 1486–1507. doi:10.1016/j.jmps.2012.04.002. http://www.sciencedirect.com/science/article/pii/S0022509612000749.

Coenen, E.W.C., Kouznetsova, V.G., Bosco, E., Geers, M.G.D., 2012. A multi-scale approach to bridge microscale damage and macroscale failure: a nested computational homogenization-localization framework. Int. J. Fract. 178, 157–178. doi:10.1007/s10704-012-9765-4.

Damanpack, A., Aghdam, M., Shakeri, M., 2015. Micro-mechanics of composite with {SMA} fibers embedded in metallic/polymeric matrix under off-axial loadings. Eur. J. Mech. - A/Solids 49, 467–480. doi:10.1016/j.euromechsol.2014.09.006. http://www.sciencedirect.com/science/article/pii/S0997753814001405.

Dvorak, G., Bahei-El-Din, Y., Wafa, A., 1994. The modeling of inelastic composite materials with the transformation field analysis. Modell. Simul. Mater. Sci. Eng. 2, 571.

Fish, J., Filonova, V., Fafalis, D., 2015. Computational continua revisited. Int. J. Numer. Methods Eng. 102, 332–378. doi:10.1002/nme.4793.

Fish, J., Kuznetsov, S., 2010. Computational continua. Int. J. Numer. Methods Eng. 84, 774–802. doi:10.1002/nme.2918.

Fish, J., Kuznetsov, S., 2012. From homogenization to generalized continua. Int. J. Comput. Methods Eng. Sci. Mech. 13, 77–87. doi:10.1080/15502287.2011.654174.

Fish, J., Nayak, P., Holmes, M.H., 1994. Microscale reduction error indicators and estimators for a periodic heterogeneous medium. Comput. Mech. 14, 323–338. doi:10.1007/BF00350003.

Fish, J., Yuan, Z., 2005. Multiscale enrichment based on partition of unity. Int. J. Numer. Methods Eng. 62, 1341–1359. doi:10.1002/nme.1230.

Fish, J., Yuan, Z., 2007. Multiscale enrichment based on partition of unity for nonperiodic fields and nonlinear problems. Comput. Mech. 40, 249–259. doi:10.1007/s00466-006-0095-0.

Forest, S., 2002. Homogenization methods and the mechanics of generalized continua–part 2. Theor. Appl. Mech. 28, 113–144.

Forest, S., Dendievel, R., Canova, G.R., 1999. Estimating the overall properties of heterogeneous cosserat materials. Modell. Simul. Mater. Sci. Eng. 7, 829.

Forest, S., Pradel, F., Sab, K., 2001. Asymptotic analysis of heterogeneous cosserat media. Int. J. Solids Struct. 38, 4585–4608.

Forest, S., Sab, K., 1998. Cosserat overall modeling of heterogeneous materials. Mech. Res. Commun. 25, 449–454.

Goli, E., Bayesteh, H., Mohammadi, S., 2014. Mixed mode fracture analysis of adiabatic cracks in homogeneous and non-homogeneous materials in the framework of partition of unity and the path-independent interaction integral. Eng. Fract. Mech. 131, 100–127. doi:10.1016/j.engfracmech.2014.07.013. http://www.sciencedirect.com/science/article/pii/S0013794414002239.

Hassani, B., Hinton, E., 1998. A review of homogenization and topology opimization ii–analytical and numerical solution of homogenization equations. Comput. Struct. 69, 719–738. doi:10.1016/S0045-7949(98)00132-1. http://www.sciencedirect.com/science/article/pii/S0045794998001321.

Hassani, B., Hinton, E., 1998. A review of homogenization and topology optimization i–homogenization theory for media with periodic structure. Computers & Structures 69, 707–717. doi:10.1016/S0045-7949(98)00131-X. http://www.sciencedirect.com/science/article/pii/S004579499800131X.

Hosseini, S., Bayesteh, H., Mohammadi, S., 2013. Thermo-mechanical xfem crack propagation analysis of functionally graded materials. Materials Science and Engineering: A 561, 285–302. doi:10.1016/j.msea.2012.10.043. http://www.sciencedirect.com/science/article/pii/S0921509312014785.

Kouznetsova, V., Geers, M., Brekelmans, W., 2004. Multi-scale second-order computational homogenization of multi-phase materials: a nested finite element solution strategy. Computer Methods in Applied Mechanics and Engineering 193, 5525–5550. doi:10.1016/j.cma.2003.12.073. http://www.sciencedirect.com/science/article/pii/S0045782504002853, advances in Computational Plasticity.

Kouznetsova, V.G., 2002. Computational homogenization for the multi-scale analysis of multi-phase materials. Eindhoven: Technische Universiteit Eindhoven Ph.D. thesis. http://repository.tue.nl/5d0651c1-b634-4c57-b8a6-682575168a0d.

Liu, W.K., McVeigh, C., 2008. Predictive multiscale theory for design of heterogeneous materials. Comput. Mech. 42, 147–170. doi:10.1007/s00466-007-0176-8.

McVeigh, C., Vernerey, F., Liu, W.K., Brinson, L.C., 2006. Multiresolution analysis for material design. Comput. Methods Appl. Mech. Eng. 195, 5053–5076. doi:10.1016/j.cma.2005.07.027. http://www.sciencedirect.com/science/article/pii/S0045782505005372. john H. Argyris Memorial Issue. Part I.

Michel, J.C., Suquet, P., 2003. Nonuniform transformation field analysis. Int. J. Solids Struct. 40, 6937–6955.

Michel, J.C., Suquet, P., 2016. A model-reduction approach in micromechanics of materials preserving the variational structure of constitutive relations. Journal of the Mechanics and Physics of Solids 90, 254–285.

Miehe, C., 2002. Strain-driven homogenization of inelastic microstructures and composites based on an incremental variational formulation. Int. J. Numer. Methods Eng. 55, 1285–1322. doi:10.1002/nme.515.

Miehe, C., Koch, A., 2002. Computational micro-to-macro transitions of discretized microstructures undergoing small strains. Arch. Appl. Mech. 72, 300–317. doi:10.1007/s00419-002-0212-2.

Mohammadi, S., 2012. XFEM Fracture Analysis of Composites. John Wiley & Sons.

Nemat-Nasser, S., Hori, M., 1998. Micromechanics: Overall Properties of Heterogeneous Materials. Elsevier, New York.

Nguyen, V.P., Lloberas-Valls, O., Stroeven, M., Sluys, L.J., 2012. Computational homogenization for multiscale crack modeling. implementational and computational aspects. Int. J. Numer. Methods Eng. 89, 192–226. doi:10.1002/nme.3237.

Oliver, J., Huespe, A., Sánchez, P., 2006. A comparative study on finite elements for capturing strong discontinuities: E-fem vs x-fem. Comput. Methods Appl. Mech. Eng. 195, 4732–4752. doi:10.1016/j.cma.2005.09.020. http://www.sciencedirect.com/science/article/pii/S0045782505005049. john H. Argyris Memorial Issue. Part I.

Rohan, E., Naili, S., Cimrman, R., Lemaire, T., 2012. Multiscale modeling of a fluid saturated medium with double porosity: relevance to the compact bone. J. Mech. Phys. Solids 60, 857–881. doi:10.1016/j.jmps.2012.01.013. http://www.sciencedirect.com/science/article/pii/S002250961200021X.

Roussette, S., Michel, J.C., Suquet, P., 2009. Nonuniform transformation field analysis of elastic–viscoplastic composites. Compos. Sci. Technol. 69, 22–27.

Sánchez, P., Blanco, P., Huespe, A., Feijóo, R., 2011. Failure-oriented multi-scale variational formulation for softening materials. Technical Report P D.

Sánchez, P.J., Blanco, P., Huespe, A.E., Feijóo, R., 2013. Failure-oriented multi-scale variational formulation: micro-structures with nucleation and evolution of softening bands. Comput. Methods Appl. Mech. Eng. 257, 221–247.

Tadmor, E.B., Miller, R.E., 2011. Modeling Materials: Continuum, Atomistic and Multiscale Techniques. Cambridge University Press.

Tang, S., Kopacz, A.M., Chan O'Keeffe, S., Olson, G.B., Liu, W.K., 2013. Concurrent multiresolution finite element: formulation and algorithmic aspects. Comput. Mech. 52, 1265–1279. doi:10.1007/s00466-013-0874-3.

Tian, R., Chan, S., Tang, S., Kopacz, A.M., Wang, J.S., Jou, H.J., Siad, L., Lindgren, L.E., Olson, G.B., Liu, W.K., 2010. A multiresolution continuum simulation of the ductile fracture process. J. Mech. Phys. Solids 58, 1681–1700. doi:10.1016/j.jmps.2010.07.002. http://www.sciencedirect.com/science/article/pii/S0022509610001316.

Tognevi, A., Guerich, M., Yvonnet, J., 2016. A multi-scale modeling method for heterogeneous structures without scale separation using a filter-based homogenization scheme. Int. J. Numer. Methods Eng.

Toro, S., Sánchez, P., Huespe, A., Giusti, S., Blanco, P., Feijóo, R., 2014. A two-scale failure model for heterogeneous materials: numerical implementation based on the finite element method. Int. J. Numer. Methods Eng. 97, 313–351. doi:10.1002/nme.4576.

Vernerey, F., Liu, W.K., Moran, B., 2007. Multi-scale micromorphic theory for hierarchical materials. J. Mech. Phys. Solids 55, 2603–2651. doi:10.1016/j.jmps.2007.04.008. http://www.sciencedirect.com/science/article/pii/S0022509607000877.

Vernerey, F.J., Kabiri, M., 2014. Adaptive concurrent multiscale model for fracture and crack propagation in heterogeneous media. Comput. Methods Appl. Mech. Eng. 276, 566–588. doi:10.1016/j.cma.2014.03.004. http://www.sciencedirect.com/science/article/pii/S0045782514000905.

Yuan, Z., Fish, J., 2008. Toward realization of computational homogenization in practice. Int. J. Numer. Methods Eng. 73, 361–380. doi:10.1002/nme.2074.

Yvonnet, J., Bonnet, G., 2014. A consistent nonlocal scheme based on filters for the homogenization of heterogeneous linear materials with non-separated scales. Int. J. Solids Struct. 51, 196–209.